Fall 2012

# Free-radical maleation of poly(butylene adipate-co-terephthalate) in supercritical carbon dioxide and its effect on the percolation and deformation mechanism of layered silicate nanocomposites

Alexandria Niemoeller



Department: Chemical and Biochemical Engineering

# FREE-RADICAL MALEATION OF POLY(BUTYLENE ADIPATE-CO-TEREPHTHALATE) IN SUPERCRITICAL CARBON DIOXIDE AND ITS EFFECT ON THE PERCOLATION AND DEFORMATION MECHANISM OF LAYERED SILICATE NANOCOMPOSITES

by

ALEXANDRIA NIEMOELLER

A DISSERTATION

Presented to the Faculty of the Graduate School of the

MISSOURI UNIVERSTIY OF SCIENCE AND TECHNOLOGY

In Partial Fulfillment of the Requirements for the Degree

DOCTOR OF PHILOSOPHY

in

CHEMICAL ENGINEERING

2012

Approved

Sunggyu Lee, Advisor

Douglas Ludlow

Joseph Smith

David Westenberg

Fatih Dogan

## PUBLICATION DISSERTATION OPTION

This dissertation has been prepared in the style utilized by the "Specifications for Theses and Dissertations" of the Missouri University of Science and Technology. Pages 1-12 have been added for introductory purposes and pages 13-35 and 36-59 will be separately submitted for publication in Polymer Engineering and Science, and 60-89 will be submitted to the Journal of Applied Polymer Science.

# ABSTRACT

The utilization of compostable polymers such as poly(butylene adipate-co-terephthalate) (PBAT) in single-use packaging applications can mitigate the water, solvents, and energy required for processing plastic waste. PBAT exhibits exceptional elongational properties, but its moderate water vapor permeability and low tensile modulus limit the applications in which PBAT can be employed. In this work, PBAT nanocomposites were produced at various loadings of organically-modified montmorillonite. The secondary structure of nanoparticles formed within the PBAT matrix was evident in the terminal region of the linear viscoelastic response under oscillatory shear, and a percolation threshold was determined to occur at 3.88% clay by weight. Transmission electron microscopy (TEM), x-ray diffraction (XRD), and the water vapor transmission rate (WVTR) were also utilized to elucidate the clay nanoparticle structure and the effect of increased clay loading on thermal and mechanical and properties was also studied.

To improve the level of clay exfoliation, a graft copolymer was developed as a compatiblizer. The maleation of PBAT was demonstrated via a solvent-free free-radical initiated grafting process in a supercritical carbon dioxide medium. The grafted anhydride moieties were modified with benzylamine to aid in FTIR and $^{1}$H NMR spectroscopy, and it was calculated that PBAT-g-MA was produced at a graft level ranging between 1.16 and 1.63%. The graft copolymer was then incorporated in PBAT nanocomposites to examine the compatibilization effects on the development of a nanoparticle network. The addition of 5% PBAT-g-MA resulted in improved clay dispersion and exfoliation evidenced through TEM, XRD, permeation analysis, and tensile testing. Differential scanning calorimetry revealed that the presence of PBAT-g-MA nucleated early onset crystallization but the organized folding of the PBAT chains was hindered by the percolated clay structure resulting in a lower overall percent crystallinity. Thermogravimetric analysis revealed that the compatibilized samples demonstrated onset degradation at lower temperatures and an increased char formation at 600°C.

# ACKNOWLEDGMENTS

I would like to express my deepest gratitude to Dr. Sunggyu Lee for his caring, guidance, and wisdom. Dr. Lee's commitment to high academic standards serves as a constant source of motivation and the environment provided to his group members could not be more conducive to excellent research. I would also like to recognize Dr. Douglas Ludlow, Dr. Fatih Dogan, Dr. David Westenberg, and Dr. Joseph Smith for their counsel as members of my doctoral committee. This work would also not have been possible without the support of the U.S. Department of Education's GAANN Fellowship and the Missouri University of Science and Technology Chancellor's Fellowship.

I would also like to express thanks to Dr. Mahin Shahlari and Dr. Jonathan Wenzel for their continued mentorship and friendship, and Barbi Wheelden for her frequent assistance in the completion of experiments and her unfaltering positive attitude no matter what difficulty we faced in the lab. Thank you to Dr. Tadashi Tokuhiro and Dr. Rex Gerald for NMR theory and operation instruction, Dr. Jeffrey Thomas for Instron training, and Sergey Vorontsov of the University of Akron for ARES operation instruction.

I would also like to thank my mother, Chris Niemoeller, for her endless love, support, and encouragement while we worked towards the completion our dissertations simultaneously. Her example has motivated me to follow a path of lifelong education, and for this (and so much more) I am forever grateful.

Special thanks go to Matt McCarthy for his optimism, patience, and constructive advice. His strength has carried me through the most difficult stage of this work. To my other family members and friends, I would have never made it through the challenging times without your best wishes and support.

# TABLE OF CONTENTS

Page

# LIST OF ILLUSTRATIONS

# LIST OF TABLES

# NOMENCLATURE

| Symbol | Description |
|---|---|
| HDT | Heat Deflection Temperature |
| MMT | Montmorillonite |
| PBAT | Poly(Butylene Adipate-co-Terephthalate) |
| PBAT-g-MA | PBAT and Maleic Anhydride Graft Copolymer |
| MA | Maleic Anhydride |
| PLA | Polylactide |
| DCP | Dicumyl Peroxide |
| $scCO_2$ | Supercritical Carbon Dioxide |
| HDPE | High-Density Polyethylene |
| LDPE | Low-Density Polyethylene |
| MFR | Melt Flow Rate |
| 30B | Cloisite 30B |
| XRD | X-Ray Diffraction |
| TEM | Transmission Electron Microscopy |
| WVTR | Water Vapor Transmission Rate |
| DSC | Differential Scanning Calorimeter |
| TGA | Thermogravimetric Analysis |
| ϴ | Angle of X-Ray Diffraction |
| MD | Machine Direction |
| G’ | Storage Modulus |
| G’’ | Loss Modulus |
| ω | Angular Frequency |
| γ | Strain Amplitude |
| η* | Complex Viscosity |

| | |
|---|---|
| Φ | Volume Percent |
| FTIR | Fourier Transform InfraRed |
| ATR | Attenuated Total Reflectance |
| NMR | Nuclear Magnetic Resonance |
| AIBN | 2,2’-Azobisisobutyronitrile |
| BPO | Benzoyl Peroxide |
| THF | Tetrahydrofuran |
| BA | Benzylamine |
| $T_g$ | Glass Transition Temperature |
| $T_m$ | Melting Temperature |
| GPC | Gel Permeation Chromatography |
| MWD | Molecular Weight Distribution |
| $T_{Ons}$ | Onset Temperature |
| $T_C$ | Crystallization Temperature |
| $t^{1/2}$ | Half Crystallization Time |

# 1. BACKGROUND

## 1.1. INTRODUCTION

As landfills and waterways become increasingly filled with plastic waste that is nearly entirely resistant to breakdown due to the effects of erosion, sunlight exposure, or attack by microorganisms, global attention is turning to the life cycle and post-consumer processing that is required for plastic products. Plastic recycling serves as a possible route for mitigating plastic waste, but can require toxic chemicals as well as a fuel source for the heating and operation of reprocessing equipment. The overall recycling and regeneration pathways generate a significant amount of carbon dioxide and other waste solvent streams. Incineration processes aid in reducing the volume of plastic waste, but also involve large fuel requirements and carbon dioxide emissions [1]. Recycling and incineration technologies will be used more widely as these technologies advance, but there still is a need for innovation in the field of biodegradable plastic materials.

Many applications exist in which biodegradable materials have found their niche, such as: food packaging and other single-use disposable items, drug delivery devices, scaffolds for engineered tissues, and agricultural films [2]. However, most commercially-available compostable polymer resins demonstrate less robust mechanical and thermal performance at a higher price than conventional plastics [3]. To realize the full potential of these biodegradable polymers and expand the applications in which they can be utilized, the incorporation of various fillers and polymer modifications have been investigated to reduce costs and improve the properties of the final products. The following collection of papers addresses the optimization of a biodegradable polymer nanocomposite through the study of the development of a nanofiller network and the

effects of this secondary phase on the barrier, rheological, thermal, and mechanical properties of the final product. This multifaceted investigation also covers the production of a compatibilizer by free radical polymer grafting in a solvent-free environment and the further incorporation of this graft copolymer into the nanocomposite in order to determine the effects on clay percolation and processability. The compatibilization of this polymer-nanofiller system is aimed at improving the barrier properties while maintaining the compostability and superior elongational properties desired for single-use packaging film.

## 1.2. POLYMER CLAY NANOCOMPOSITES

The first documented report on clay nanocomposites was published in 1993 by the Toyota Research and Development Lab in Japan in 1993 [4]. Upon reporting the improved strength, modulus, and heat deflection temperature (HDT) of the composites prepared with less than 5 weight percent montmorillonite (MMT), the research done in this area grew exponentially over the next few decades. The large aspect ratio of the clay particles as well as the high surface area provide for increased interfacial interactions and stress transfer between phases. Montmorillonite is one of the most widely-studied layered silicates which has been shown to exhibit favorable swelling properties and can thus be relatively easily modified and tailored for a particular polymer matrix. Therefore, the remainder of the discussion will focus on this particular nanoclay.

Montmorillonite, a 2:1 phyllosilicate, is one of the most commonly-used nanoclays in polymer-layered silicate nanocomposites due to its low cost, wide availability and its high surface area-to-volume ratio. The oxides present on the highly reactive surface cause the individual lamellae of MMT to have a slightly negative charge

that attracts cations such as $Na^{+}$ and $Ca^{2+}$ [5]. The system of weak forces between the clay platelets and the sorbed cations induce the platelets to orient and aggregate into structured clay tactoids, but this lamellar structure of MMT can be swelled relatively easily in solution or a polymer melt [6].

To promote the separation of the clay lamellae and expose more surface area of the MMT, the sorbed cations are often exchanged with cations with larger functional groups. The spacing between organically-modified clay platelets, or d-spacing, is larger than unmodified MMT and this has been shown to further increase clay platelet exfoliation during nanocomposite preparation [7-9]. Nanocomposites prepared with modified clays typically exhibit improved barrier, thermal, and mechanical properties at lower clay loading level. Polymer-layered silicate nanocomposites have been shown to have improved heat deflection temperatures, flame retardancy, as well as dimensional stability [10, 11]. A wealth of research has been carried out to determine the optimal clay modification for a particular polymer matrix to ultimately develop lightweight, inexpensive composite materials with tailored properties; however, limited research is available on newly developed biodegradable polyesters such as poly(butylene adipate-co-terephthalate).

### 1.3. POLY(BUTYLENE ADIPATE-CO-TEREPHTHALATE)

The particular compostable polymer chosen for this investigation was poly(butylene adipate-co-terephthalate) (PBAT), a biodegradable thermoplastic with exceptionally good elongational properties, optical properties and wear-resistance. These characteristics makes this aliphatic-aromatic copolyester the only commercially-available compostable resin with properties similar to high-density polyethylene and it is

correspondingly used in many film applications in food packaging and agricultural and landscaping products. Figure 1.1 gives the structure of this random copolymer of butylene adipate and butylene terephthalate residues. By altering the ratio of butylene adipate and butylene terephthalate monomers during polycondensation, this random copolymer can display a range of thermal and mechanical properties as well as biodegradation rates. Commercial grades of PBAT has been shown to degrade readily in the presence of enzymes found in a compost environment within a few weeks, however the limited barrier properties of PBAT films limit the applications in which it can be used [12, 13].

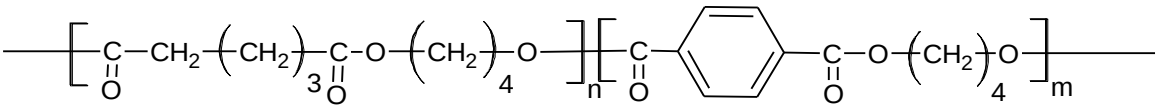

Figure 1.1. PBAT Structure

As clays such as MMT are naturally-occurring and environmentally-friendly, they also serve as ideal nano-scale fillers for any biodegradable polymer. For PBAT nanocomposites in particular, the clay structure developed through melt compounding must be evaluated to ensure that the processing characteristics of PBAT that make it such a promising biodegradable material are retained. The development of structure-property relationships and an estimation of the optimal clay loading for PBAT film applications is the first step to widening the applications for PBAT nanocomposites.

## 1.4. PERCOLATION THEORY

A composite is considered to be percolated when there is a secondary network of particles within the host matrix and a connected pathway is created from one side through to an opposing face of the material. While the discussion of nanocomposite percolation is pertinent to layered silicate-filled polymers, percolation threshold estimation has been most widely researched in the field of electrically conducting blends and films with carbon black, carbon nanotubes/nanowires, graphite, and graphene [14-18]. This connected pathway demonstrated in Figure 1.2 can improve the thermal and electrical conductivity in composites with carbon-based nanofillers while simultaneously aiding in strengthening and stabilizing the material.

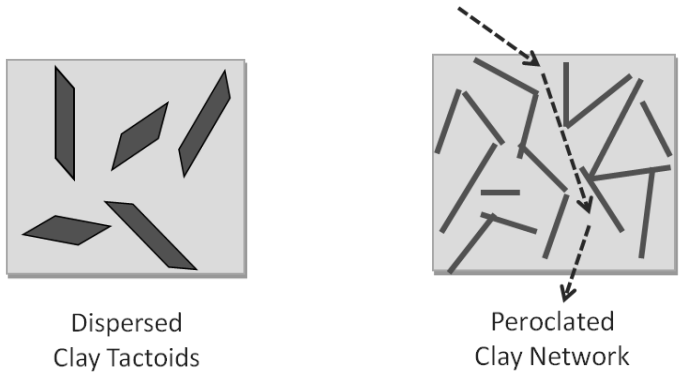


Figure 1.2. Percolated Structure of Exfoliated Clay Platelets

The intention of identifying the specific percolation threshold for a particular polymer/filler system is to estimate the minimum amount of filler material that is required for the target improvement in electrical, barrier, thermal, or mechanical properties. Beyond this percolation threshold, the final product may be more expensive and difficult to process due to an elevated viscosity and more brittle nature. At elevated concentrations, the nanoparticles can aggregate and cause heightened localized stress

near large tactoids and this non-uniform behavior can ultimately lead to early failure under deformation.

## 1.5. MALEATION OF POLYMER RESINS

The polymer grafting technique called maleation is one of the most widely practiced and reviewed polymer modification methodologies with over 30 years of publications available for review [19]. The many structural analogues of maleic anhydride (MA) show a broad range of reaction pathways and the attachment of this multi-functional moiety to the backbone of thermoplastic materials can augment the polarity, reactivity, and surface energy of these polymers. MA-grafting and copolymers have been in a wide range of applications, including: improved hydrophilicity of polymer substrates for producing biocompatible materials which support cell adhesion [20-22], enhanced dispersion of fillers and nanoparticles [23-27], and compatibilization of immiscible polymer blends [28, 29].

MA grafting has been demonstrated in many reaction media and with various types of free radical initiators. The sections that follow summarize the most commonly-used techniques as well as recent innovation related to MA grafting.

## 1.6. POLYMER GRAFTING METHODS

**1.6.1. Melt Grafting.** A relatively simple method for the modification of polymer resins involves the incorporation the desired additives and free radical initiators in a polymer melt. The thermal degradation of the initiator generates a radical which can abstract hydrogen from the polymer backbone. The generated macroradical goes on to form bonds with the free monomer that is co-fed to the system. The major benefit of this

process is that it utilizes existing compounding and extrusion equipment with minimal modifications to the established feeding, collection, and cleaning procedures. Reactive processing can thus be carried out continuously and can also be utilized directly while compounding polymers and nanofillers. Further, extrusion grafting has been shown to reduce interfacial tension between the polymer phase and filler surface as well as in polymer blends [30].

The most significant drawback of melt grafting is the effect that free radical initiators such as peroxides have on the molecular weight and extent of cross-linking in the final product. The radicals generated on the polymer backbone can alternatively form carbon-carbon cross-linking bonds and extended extrusion time or heightened peroxide activity have been shown to increase the overall cross-linking and gel fraction of the product [31]. The reactive processing of polylactide (PLA) and PBAT above 0.7 parts per hundred (phr) of added dicumyl peroxide (DCP) generated “gel-like components” which destabilized and disrupted the extrusion process [30]. Further, the PLA/PBAT processed with up to 0.5 phr displayed minimally improved mechanical properties and above 0.5 phr DCP the blends had a reduced elongation at break, tensile modulus and tensile strength.

Another challenge associated with reactive extrusion is that it is dependent upon the diffusion of the radical and monomer through the highly viscous polymer melt. This slow diffusion rate heightens the likelihood of free radical recombination or homopolymerization of the added monomer [32]. During reactive extrusion the monomer and initiator typically exhibit melting prior to the macromolecule and can be segregated as a separate immiscible phase dispersed throughout the polymer in the first

few sections of the extruder [33]. These “cages” of locally high concentrations of initiator can generate hot spots of enhanced polymer degradation and preferential grafting in only those regions. This cage effect has a detrimental effect on product quality, lowering the grafting efficiency and producing a polymer containing excess monomer with a reduced average molecular weight.

Surprisingly, this so-called solution-free process is often followed up with an extraction process to remove unreacted monomer and spent initiator from the extrudate. If not, the presence of residual free monomer and initiator can migrate and further react if the product is heated a second time or simply during storage at ambient conditions further reducing the polymer viscosity [33].

**1.6.2. Free Radical Grafting in Solution.** Many polymer grafting reactions are carried out in a liquid solution instead of directly in an extruder or batch mixer. This helps to reduce the initiator cage effects as the viscosity of the reaction medium is greatly reduced as compared to a molten polymer. It has been reported that the probability of a free radical pair escaping the polymer cage was found to be significantly lower in the solid polymer phase (0.01-0.1) than in a liquid solution (0.3-0.8) [34]. However, the low local concentrations of reactants can limit graft levels and increase the reaction time required. Another key issue with solution grafting is the solvent requirements and post-reaction purification steps. A solvent in which the polymer dissolves fully must first be found, and a second solvent must be used to precipitate and wash the graft-copolymer. This type of solvent/antisolvent system can be particularly difficult to find for biodegradable polymer at a reasonable cost. Additionally, the monomer and initiator must also be soluble in both selected solvents. The overall process requires a significant

amount of expensive and generally toxic chemicals which can then limit the applications in which the product can be used.

**1.6.3. Radiation-Induced Grafting.** Polymer grafting through the irradiation of a polymer substrate with gamma or UV rays in the presence of the desired grafting moiety can be conducted without toxic solvents. The foremost reason that this method is not commonly used is that the radicals are only generated on the surface of the polymer and the graft level is extremely low [35, 36]. This grafting technique has still proven useful in the surface modification of many forms of polymer surfaces: films, porous scaffolds, powders, etc. Surface properties such as hydrophilicity, printability, and biocompatibility can be rapidly altered, albeit to a very low extent.

**1.6.4. Supercritical Carbon Dioxide as a Free-Radical Grafting Medium.** Carbon dioxide is an inexpensive, freely available chemical which displays comparatively low critical properties (a critical temperature of 31.1°C and a critical pressure of 7.39 MPa). Figure 1.3 displays a generic phase diagram for a pure species such as carbon dioxide where above both the critical temperature and pressure, it becomes a supercritical fluid and displays the combined properties of a liquid and a gas. Supercritical carbon dioxide ($scCO_2$) displays liquid-like density and solvent power but the low viscosity of a gas. This heightened solvent power and reduced viscosity essentially eliminates the initiator cage effects observed in melt and solution grafting [37]. It also serves as an excellent heat transfer medium that has a solvent density which can be easily tuned for a particular application by varying the temperature and pressure, particularly near the critical point [38].

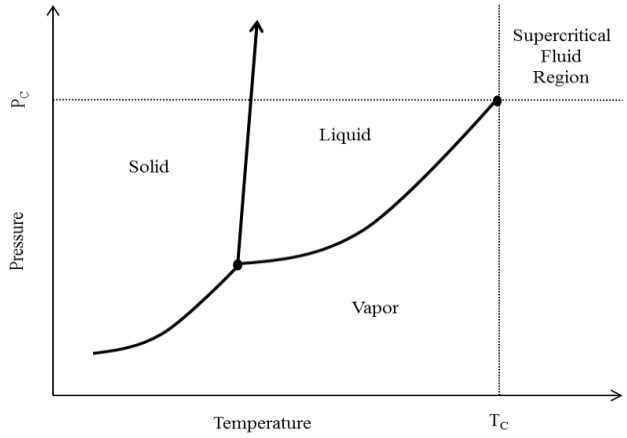


Figure 1.3. Phase Diagram for Pure Species

While $scCO_2$ is used commonly in processes such as the decaffeination of coffee and the extraction of chemical and medicinal components from temperature or pressure sensitive substances, it also functions as an effective medium for the processing and production of polymeric materials. With the exception of amorphous fluoropolymers and silicones, most polymers are not dissolved by $scCO_2$ and instead are swelled significantly. This is particularly true in polymers with a low level of crystallinity, such as PBAT, as $scCO_2$ has been shown to diffuse primarily through the amorphous regions of a polymeric material. PBAT displays a high level of $scCO_2$ sorption and plasticization, making it a prime candidate for supercritical fluid processing [39].

Avoiding the dissolution of the polymer chain itself also ensures that the reaction medium maintains a lower viscosity than that of polymer melts or liquid polymer solutions, thus reducing mass transfer limitations. This encourages the transport of smaller molecules into the polymer and increases the polymer surface area available for grafting, providing for a higher graft level than radiation-initiated surface grafting. These

combined properties provide for a reaction medium that readily dissolves free-radical initiators, many monomers, and other functionalities that are typically affixed to a polymer backbone [40]. Further, upon a rapid depressurization or direct flow of $scCO_2$ the unused monomer and initiator can easily be removed from the reactor system without product washing and drying [41].

The use of $scCO_2$ as a reaction medium for biodegradable polymers also provides much milder processing conditions than melt or solution grafting: lower temperatures, minimal to no use of organic solvents or anti-solvents, and no appreciable degradation as compared to the high shear of melt processing equipment. This helps to ensure that the viscosity and molecular weight of the final product are not altered significantly from the resin utilized. Supercritical fluids have also been used to create microporous structures from biocompatible polymers for engineered tissues such as bone scaffolds. These processes could ultimately be combined to simultaneously modify the surface properties and microstructure of biodegradable polymers for biomedical applications.

Although there are a multitude of benefits to using $scCO_2$ for biodegradable polymer processing, limited studies have been conducted in the area of supercritical polymer grafting onto biodegradable materials. The following work focuses on the development of a graft copolymer in $scCO_2$ and its further use as a compatibilizing agent in PBAT layered silicate nanocomposites.

# 2. PERCOLATION THEORY AND DEFORMATION MECHANISM OF POLY(BUTYLENE ADIPATE-CO-TEREPHTHALATE) LAYERED SILICATE NANOCOMPOSITES

## 2.1. INTRODUCTION

Polymer reinforcement at the nano-scale level can improve the modulus, gas barrier properties, heat deflection, and flame retardancy while also controlling the crystallization and degradation rate of the composite. Nanoclay can provide these enhancements at a loading level of less than 5 weight percent. The key to optimal property improvements is achieving delamination of the layered structure producing nanofillers with aspect ratios of up to 1000 [42-48].

As with any filler material, the main challenge to producing a product with uniform properties and performance is the controlled dispersion of the nanomaterial within the matrix. While there are many methods to characterizing polymer nanocomposites, a holistic study of the dispersion state of the nanofiller includes microscopy and x-ray diffraction patterning with thermal, rheological, and mechanical testing. These methods combined give insight to how the meso-scale properties are affected by the localized development of a nanofillers network structure, and ultimately help to optimize the elements, quantities, modifications, and preparation methods for developing a nanocomposite for a specific application.

## 2.2. PERCOLATION THEORY IN POLYMER NANOCOMPOSITES

The percolation threshold of a layered silicate nanocomposite is defined as the clay loading at which a connected network is created between neighboring particles and the interactions between these particles lead to an overall change in the viscoelastic,

mechanical, and electrical properties of a material. Revealing the percolation mechanism of a particular polymer-clay system through morphology and rheology of nanocomposites at various clay loadings helps to quanttify the percolation threshold of a particular polymer-clay system and define structure-property relationships for the prediction of nanocomposite product performance.

## 2.3. PBAT NANOCOMPOSITES

Poly(butadiene adipate-co-terephthalate) (PBAT) is a biodegradable thermoplastic with exceptionally good elongational properties. This characteristic makes the aliphatic-aromatic copolyester the only commercially-available compostable resin with properties similar to HDPE and LDPE and it is correspondingly used in many single-use film applications such as food packaging and agricultural and landscaping products. As PBAT is used in biodegradable packaging, the addition of a nanofiller such as a layered silicate may be of interest to improve its barrier, thermal and mechanical properties.

## 2.4. MATERIALS AND EQUIPMENT

The PBAT used in this work was Ecoflex® F BX 7011 supplied by BASF with a density of 1.25 g/cm$^3$ and a melt flow rate (MFR) of 2.50-4.50 grams per 10 minutes at 190°C. The nanoclay compounded with the PBAT was purchased from Southern Clay under the name Cloisite 30B. The organic modification carried out on this particular MMT clay is an ion-exchange reaction with the following quarternary ammonium:

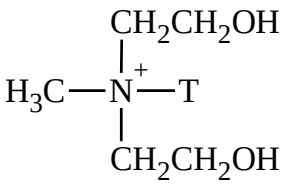

where T is tallow. At a modifier concentration of 90 meq/100g clay, this bulky organic modification gives Cloisite 30B a relatively larger d-spacing between the clay layers and it has been theorized that this results in a good level of clay exfoliation in nanocomposites [49]. This has been found to be particularly true in host matrices such as PBAT with polar pendant groups.

Compounding was performed with a Brabender co-rotating conical twin screw extruder with an L/D of 8 and a screw diameter of 42 mm. Prior to extrusion, both the clay and polymer pellets were dried under vacuum at 50°C for 24 hours. The three heating zones of the extruder were maintained at 145, 145, and 149°C from feeding zone to the die, and the feeding zone was chilled to approximately 10.4°C with a recirculating bath to prevent premature softening of the PBAT pellets. Post-extrusion, the drawn fibers were cut into pellets and pressed into testing specimens with a Carver press and 1 mm molding apparatus. Films were also drawn from the same extrusion equipment, with an average film thickness of 0.15 mm.

## 2.5. ANALYSIS METHODS

X-ray diffraction (XRD) patterns were captured using a PANalytical X'Pert PRO MRD with a copper anode, a wavelength of 0.154 nm, and a divergence slit of 0.05 mm. The diffractograms were captures from $1^\circ < 2\Theta < 10^\circ$. The imaging of the structure of the clay in PBAT was carried out with a JEOL JEM-1400F transmission electron microscope (TEM). To produce specimens thin enough for TEM imaging, the extrudate pellets were first sectioned with an ultramicrotome.

Water vapor transmission rates (WVTR) through the prepared nanocomposite films were studied according to ASTM-E96/E96M-10. Films (0.14 +/- 0.1 mm thick)

were secured to glass containers which were filled with an 8-mesh desiccant and then sealed. The testing chamber was maintained at 26°C and 52% humidity throughout the testing period, with a constant air velocity provided by a fan. The weight of each sample was taken every 12 hours over a four-day period and adjusted relative to the weight change of a prepared "dummy" sample without desiccants in the container. The water vapor transmission through the samples was then averaged from three film samples of each clay loading level.

The rheological response of the prepared composites was studied on both an ARES and ARES-G2 rheometer (TA Instruments) in the 25 mm diameter parallel plate and rectangular torsion configurations. Specimens were cut into 25 mm diameter circles and 12x25 mm specimen from 1 mm thick compression molded sheets.

Thermal analysis was carried out with a differential scanning calorimeter (DSC), DSC-Q2000 (TA Instruments), in order to characterize the glass transition, crystallization, and melting behavior of the nanocomposites. The effect of the clay loading on the degradation of the composites was investigated with an SDT-Q600 (TA Instruments) which carries out simultaneous thermogravimetric analysis (TGA) and DSC measurements. Ultra-high purity nitrogen was used in all analyses and a purge flow rate of 50 and 200 mL/min was used for the DSC-Q2000 and SDT-Q600, respectively.

The mechanical properties of the prepared composites were compared through tensile testing with a universal testing machine Instron 4469 and a TA.XT.Plus texture analyzer according to ASTM D638. A type IV dumbbell specimen and a crosshead speed of 10 mm/s was used for the Instron analysis, and a Type V specimen with a crosshead speed of 2.5 mm/s was used for all texture analysis.

## 2.6. RESULTS AND DISCUSSION

**2.6.1. X-Ray Diffraction Patterning.** X-ray diffraction patterns of neat PBAT, pure clay, and 3 and 5 wt% composites are shown in Figure 2.1. The characteristic peak of the pure clay appears at $2\theta = 4.75$; and when compounded with PBAT, this peak shifts to approximately 2.25 in the 5 wt% composite and nearly disappears in the 3 wt% sample. The reduction in height and shift of the peak is often attributed to the reduction of the average d-spacing between the clay layers which can be accomplished by the successful intercalation of the polymer chain into the interlayer gallery and/or exfoliation of the individual clay layers. While the disappearance of the characteristic clay peak does not always indicate full exfoliation, this is one method to determine if full or partial delamination of the clay has been achieved through melt compounding [50-52].

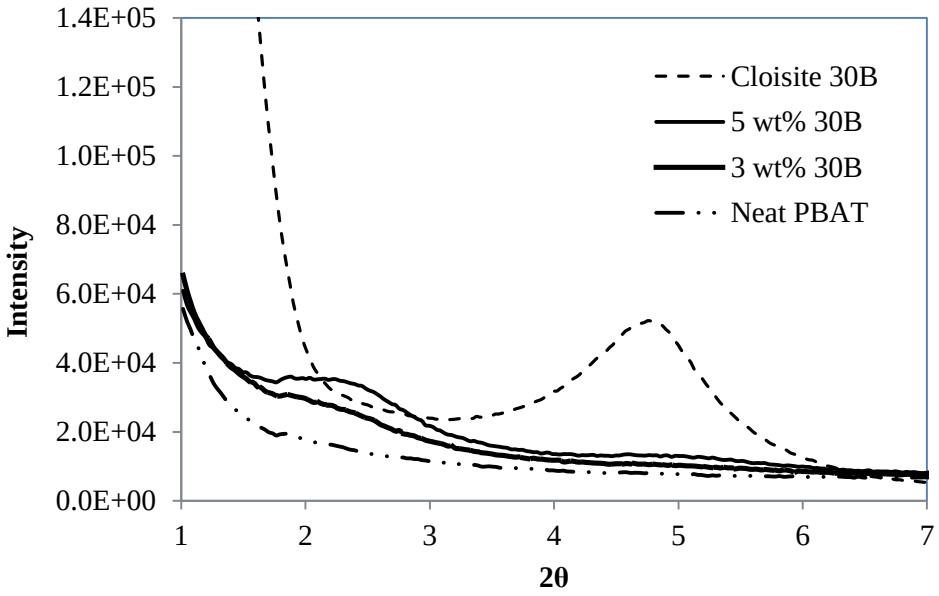


Figure 2.1. X-Ray Diffractogram of PBAT Nanocomposites

**2.6.2. Transmission Electron Microscopy.** A secondary method that is often used in conjunction with x-ray diffraction to examine the dispersion and exfoliation level of the clay phase is electron microscopy. Transmission electron microscopy (TEM) gives a nano-scale view of prepared nanocomposites so that the structure of the clay network can be viewed directly. While it cannot be assumed that the clay structure in a single TEM image is consistent throughout an entire sample, a set of multiple TEM images capturing similar results can give insight to the development of a network of clay particles. It is generally assumed that a significant level of clay exfoliation has been achieved if multiple TEM images display exfoliated clay layers along with a reduction and/or shift in the characteristic XRD peak of the clay.

In Figure 2.2, the images of the PBAT-30B nanocomposites captured using a transmission electron microscope are given for moderate and high levels of clay. At all clay loadings analyzed, individual clay platelets and partially exfoliated clay particles of 2-3 layers can be identified. In terms of the formation of a fully developed secondary network of clay, the 4 and 5 wt% composites show moderate interactions between the clay particles but the 7 wt% composite appears to the lowest loading level where the majority of clay platelets/tactoids are in direct contact with a neighboring clay particle. As the clay loading is increased, however, the number and size of visible tactoids also increases. At 15 wt% clay, the composite exhibits a high level of aggregated clay which can ultimately hamper the performance of the composite and lead to localized stresses and early failure under tension.

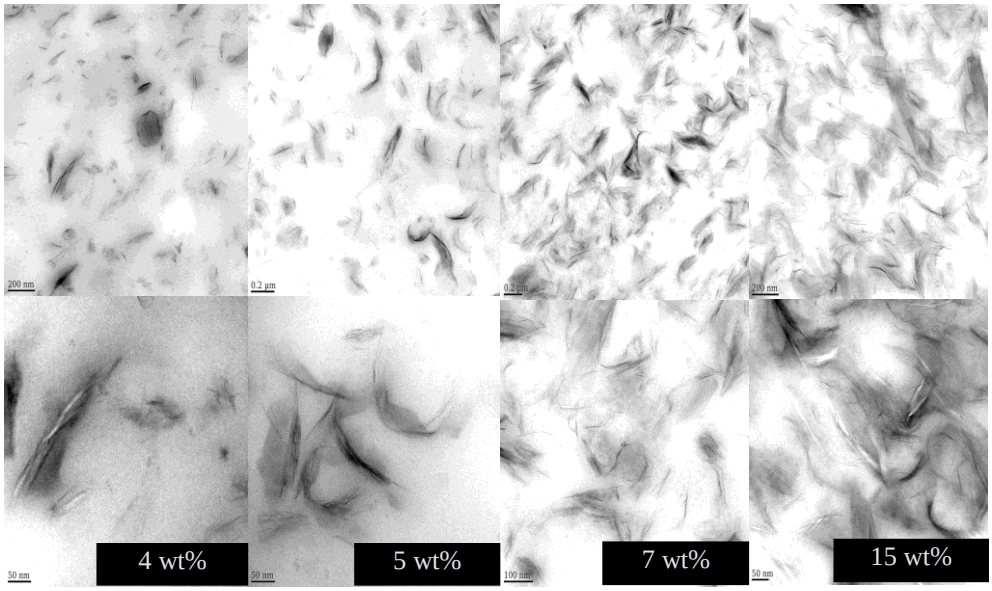


Figure 2.2. TEM Images of PBAT-30B Nanocomposites at Various Clay Loadings Magnification Scale: 200 nm (Top), 50 nm (Bottom)

**2.6.3. Water Vapor Transmission.** Another analytical method which can indirectly serve as an indication of a well-developed clay network is the study of the permeation of molecules through a composite. This is particularly of interest in materials such as PBAT which is used in film packaging of perishable items. During film extrusion, nano-scale layered materials are oriented in the machine direction (MD) and are thus perpendicular to the direction of diffusion through the films. This clay orientation has been shown to increase the tortuosity of the path of water vapor and oxygen molecules and reduce the overall permeability of the film [52-54].

While the barrier properties of a clay nanocomposite are improved as the amount of exfoliated clay layers is increased, any large tactoids or clay aggregates can cause micro-scale holes and tears in the film which can hamper the overall permeability. This would indicate that there is an optimal clay loading to produce an exfoliated clay network

with minimal aggregates. It is theorized that this clay loading is near the percolation threshold of the nanocomposite which is unique to the polymer matrix and modified clay examined. By examining the water vapor transmission rate of a set of nanocomposite films, it should be possible to identify where the clay network becomes fully percolated and above what clay loading the barrier properties of the composite are hindered.

The water vapor transmission rate through extruded PBAT-30B films was measured and compared to neat extruded PBAT film in Figure 2.3. With as little as 1 wt% 30B, the water vapor transmission rate was reduced by 29%, demonstrating the substantial improvement in barrier properties that can be realized with the incorporation of a small amount of layered silicate. This transmission rate is reduced by an additional 12.9% upon increasing the clay level to 2 wt%. At 5 wt%, however there is no additional decline in transmission rate; in fact, the average value of the three samples measured is slightly higher than that of the 2 wt% films studied. This inquiry indicates that the percolation of the clay network occurs between 2-5 wt% and the optimal barrier property improvement is attained within this range.

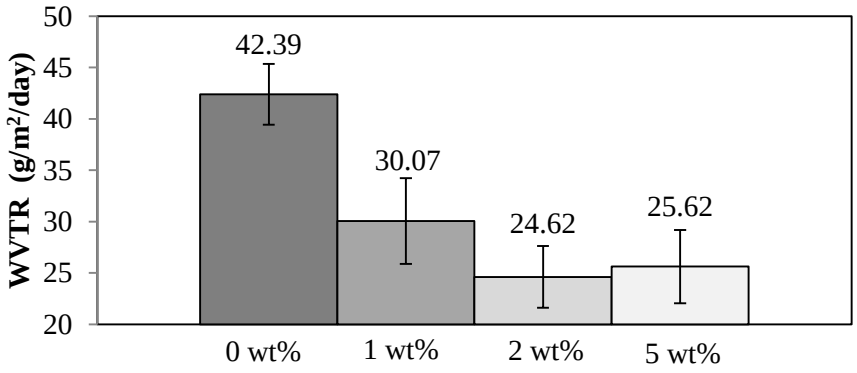


Figure 2.3. Water Vapor Transmission Rate through PBAT Nanocomposite Films above and below the Theoretical Percolation Threshold

**2.6.4. Rheological Properties.** The viscoelastic response of a composite is commonly used to study the overall processability of the material, and can also be used to investigate the structure of a nanocomposite. Rheological data, particularly in the low frequency region, can reveal whether the nanoparticles have formed a fully percolated structure within the polymer matrix.

To ensure that all rheological measurements were performed in the linear viscoelastic region of the PBAT nanocomposites, a strain sweep was carried out from an amplitude of 1 to 10%. This test was carried out at a temperature of 145°C and a frequency of 1 rad/s. Figure 2.4 shows the linear relationship of the storage and loss modulus (G' and G") throughout the entire strain range chosen. Therefore, any strain value in this range can be selected for rheological testing and a strain amplitude of 3% and a temperature of 145°C was chosen for all further analysis.

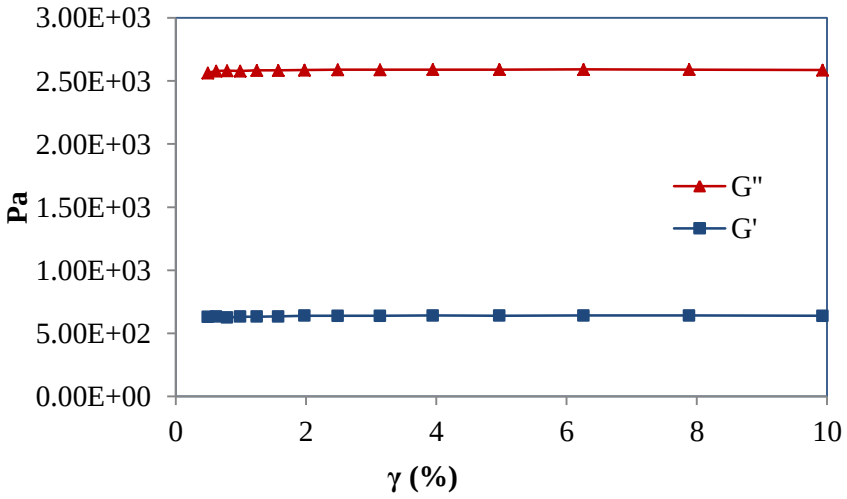


Figure 2.4. Strain Dependence of G' and G'' at ω = 1 rad/s and T = 145°C

Figures 2.5 and 2.6 show G' and G" of the prepared nanocomposites as the clay loading was increased from 3% by weight up to a maximum of 15 wt%. Composites were also prepared of 1 and 2 wt% composites, but the rheological measurements of these samples are not included in these images as they were not found to be significantly different than that of the neat PBAT. From previous work on similar polyester-clay systems, the composites above 3 wt% are expected to be above the percolation threshold of a polymer clay nanocomposite [49]. Correspondingly, the low frequency plateau of G' is visible in all composites above this assumed percolation threshold value.

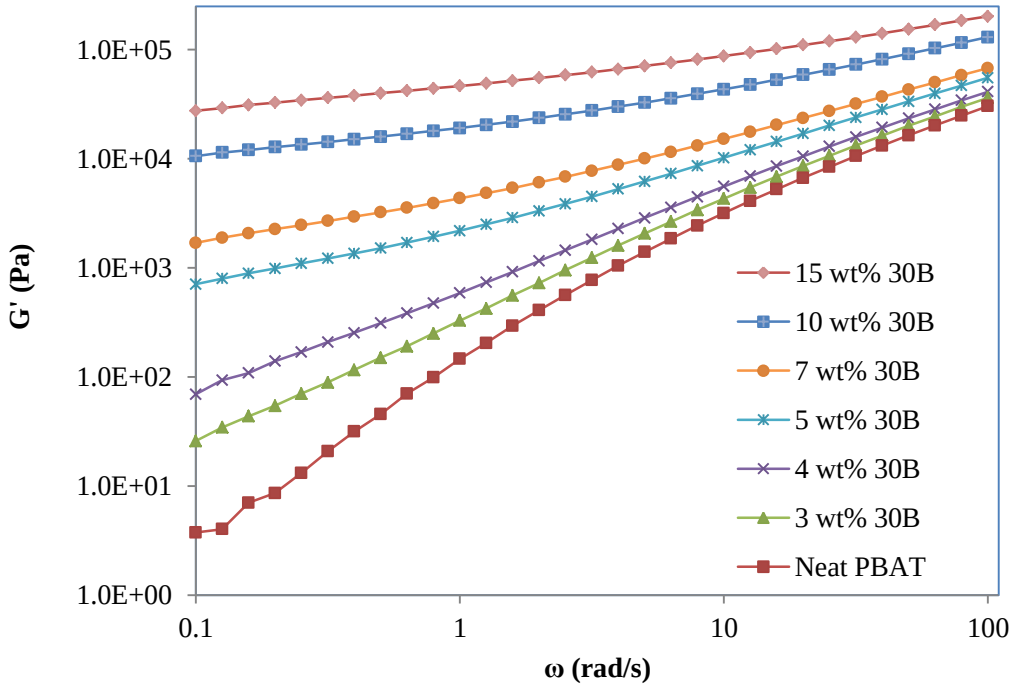


Figure 2.5. Storage (G') Modulus of PBAT Nanocomposites at Various Clay Loading Levels

To more clearly demonstrate the effect the increased clay percentage has on the viscoelastic response of PBAT, Table 2.1 gives the relative slope of the low frequency region of G' and G" for each clay loading. As the filler level is increased and the relative slopes decrease, the G' and G'' curves become less dependent on frequency of the applied strain. At 15 wt% clay, the relative slope of 0.135 signifies that the material's viscoelastic response is nearly independent of frequency. The large drop in the slope of G' between 4 and 5 weight percent is particularly worth noting, as it may signify that the development of a percolated clay network occurs near this range, resulting in a more solid-like response from the particle-particle frictional interactions as well as the polymer entrapments within the clay particles [48].

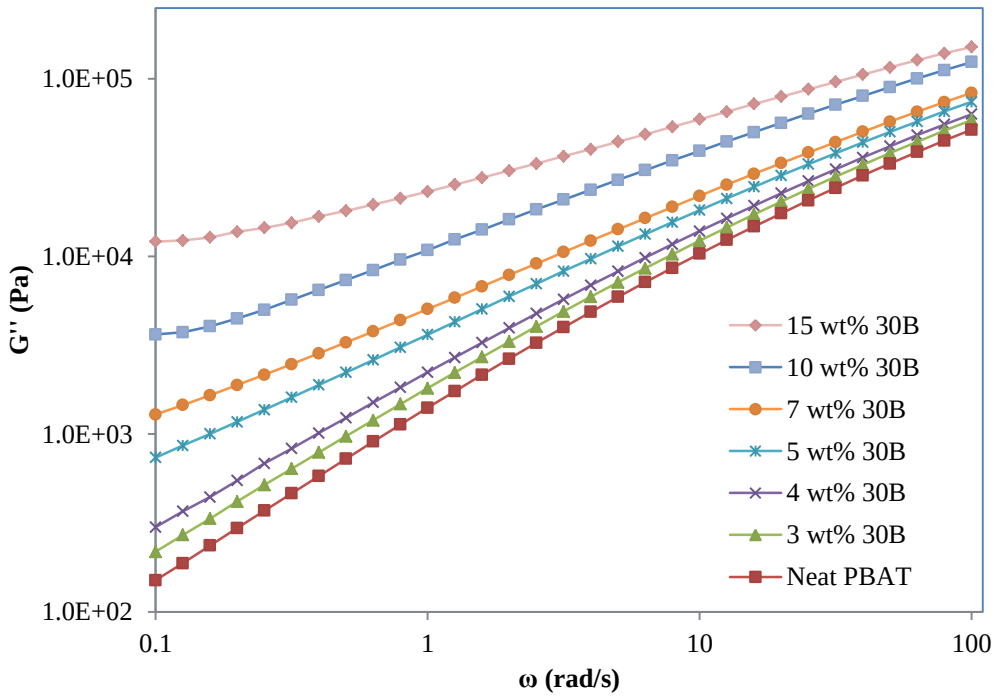


Figure 2.6. Loss Modulus (G") of PBAT Nanocomposites
at Various Clay Loading Levels

Table 2.1. Relative Slopes of G' and G" with Increased Clay Loading

| Clay Loading | Slope of G'(ω) | Slope of G''(ω) |
|---|---|---|
| Neat PBAT | 1.000 | 1.000 |
| 3 wt% 30B | 0.600 | 0.946 |
| 4 wt% 30B | 0.544 | 0.898 |
| 5 wt% 30B | 0.289 | 0.711 |
| 7 wt% 30B | 0.239 | 0.527 |
| 10 wt% 30B | 0.151 | 0.513 |
| 15 wt% 30B | 0.135 | 0.300 |

When the secondary network of particles has been established in a clay matrix, the solid-on-solid interactions dominate the viscoelastic response until the frequency of the strain applied to the composite is raised. When the frequency passes a certain value, the structure of clay platelets is not preserved and the dominant response becomes that of the polymer matrix [48, 55, 56]. This can be observed in Figure 2.7 where a crossover frequency has been identified for a 7 wt% 30B composite. Below a frequency of 0.591, the measured G" value (which correlates to the dissipation of stress through a material) is less than that of the G' value, which is associated with the elastic response to shear stress. Above this crossover frequency the structure is destroyed and the viscoelastic response of PBAT is restored. Figure 2.8 expounds upon this idea by showing the large increase in complex viscosity of the composites with increased 30B, but this effect is minimized as the frequency is increased and the clay structure is broken down through shear-thinning.

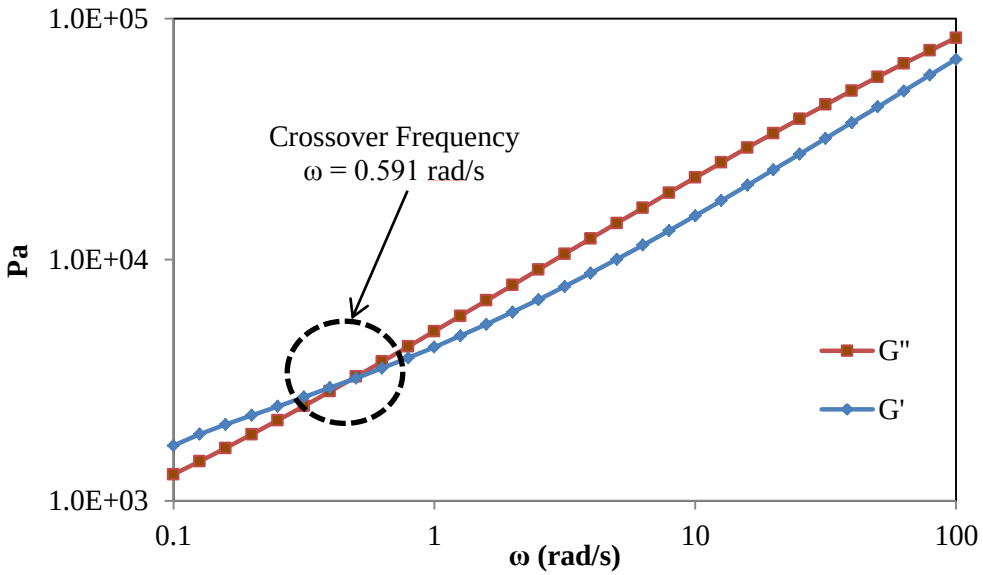


Figure 2.7. Identification of Crossover Frequency in a PBAT Composite with 7 wt% Cloisite 30B

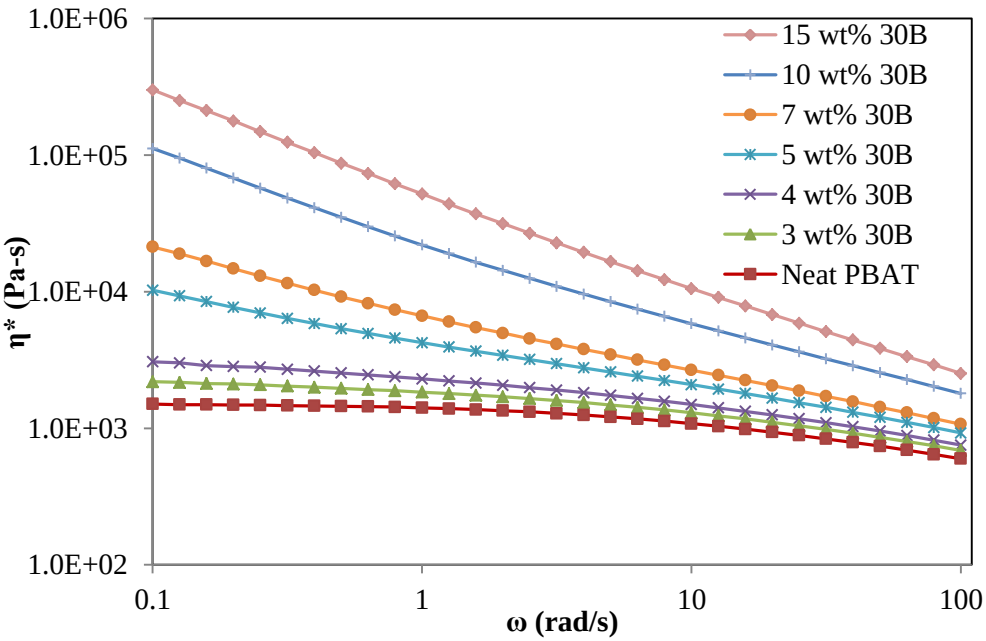


Figure 2.8. Complex Viscosity at Various Clay Loadings

The visual inspection of the effect that exfoliated nanoclay has on G', G", and the complex viscosity is an excellent tool to characterizing the level of exfoliation achieved within the PBAT matrix, however it is difficult to calculate a theoretical percolation threshold from Figures 2.4-2.8 alone. To quantitatively estimate a concentration of clay where a percolated clay network begins to form, G' was plotted against the volume percent of clay in each sample at a selected low frequency value of 0.158 rad/s in Figure 2.9. The volume percent from the intersection of the two linear relations was found to be 1.73 volume percent or approximately 3.88 weight percent, which is in line with prior publications for other polymer-clay systems prepared through melt compounding.

**2.6.5. Mechanical Properties.** The next step of the characterization of the PBAT nanocomposites was to determine how the development of the secondary clay network affected the tensile properties of the elastomer-like polymer matrix. PBAT is highly tear-resistant and the particular grade used in this work is capable of stretching more than

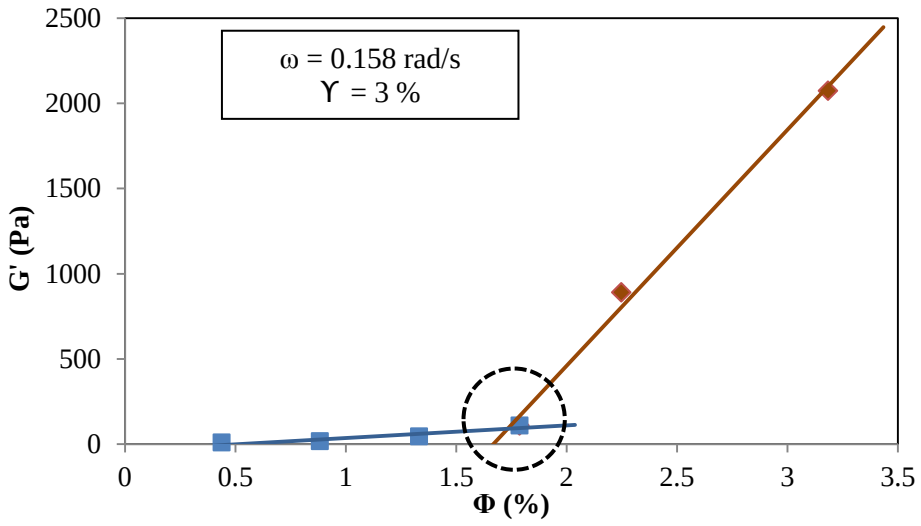


Figure 2.9. Estimating the Percolation Threshold from G' Values at Low Frequency

seven times its length before break. As the inclusion of fillers can make a polymer significantly more prone to brittle failure, the effects of compounding clay with PBAT must also be examined through tensile testing.

The improvement in the tensile modulus of the PBAT nanocomposites can be seen in Figure 2.10. A clear enhancement of the Young's modulus of the composite is shown with increasing clay percentage. The modulus can be increased by 22% with only 5 wt% clay and 52% with 10 wt% clay. It is clear through mechanical testing, that an improvement in the tensile modulus can be achieved through the incorporation of nanoclay without entirely sacrificing the favorable elongational properties of PBAT if the composite is melt compounded at a clay percentage which marginally exceeds the onset of percolation.

Figure 2.11 shows the average reduction of elongational properties as the clay loading is increased, as expected. What should be noted, however, is that even up to 3 wt% the elongation at break is not significantly lower than pure PBAT and over 450% elongation at break is achieved at as high as 10 wt% nanoclay. While there is a reduction in elongational properties with the melt compounding of nanoclay into PBAT, it is apparent that the material remains highly elastic with the incorporation of less than 10 wt% of this specific nanoclay.

The relatively large drop in elongation at break at 4 wt% is worth discussing, as it mirrors the trend found through melt rheology analysis. The percolation of the clay network alters the localized stress transfer mechanism of the polymer chains and can have a considerable effect on the tensile properties of the composite.

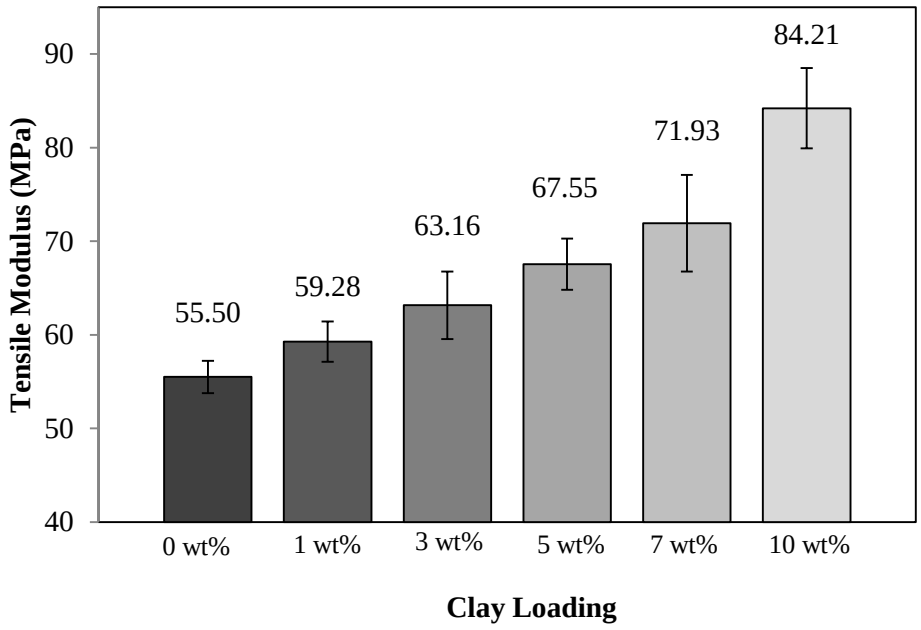


Figure 2.10. Increased Tensile Modulus with the Incorporation of Cloisite 30B

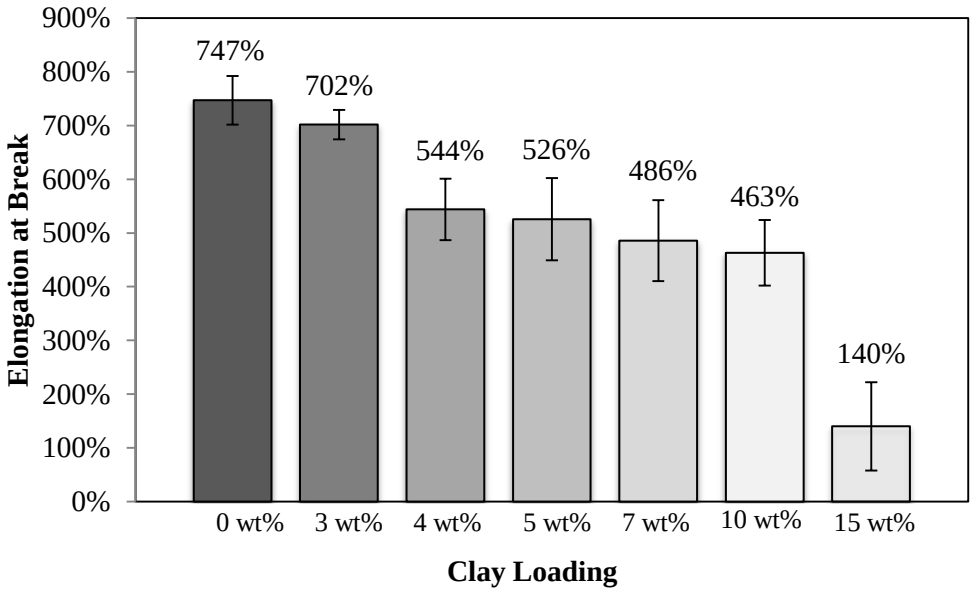


Figure 2.11. Effect of Clay Loading on Elongational Properties of PBAT Nanocomposites

**2.6.6. Thermal Analysis.** The crystallization and degradation behavior of a polymer can be altered considerably with the inclusion of nano-scale materials. For semicrystalline polymers in particular, nanoclay has been shown to facilitate crystallization as a nucleating agent, but at high concentrations the assembly of exfoliated layers into an ordered structure can hinder the chain folding and crystallization [57].

Figure 2.12 depicts the DSC cooling curves of PBAT-30B nanocomposites from 0-15 wt% at a cooling rate of 5˚C/min. Both the peak and onset temperature of crystallization is shown to increase with increased clay percentage. It is theorized that the presence of clay particles induces early crystallization by acting as a nucleating agent and aiding in localized crystal formation. The area under the crystallization curve follows an opposite trend and decreases as additional clay in compounded in PBAT. The measured enthalpy associated with this transition is related to the percent of crystallinity in the sample; therefore, a decrease in this value indicates that the high aspect ratio clay platelets and tactoids hinder the segmental free motion and disrupt the ordered stacking of the polymer chains. This forms an interesting dichotomy between the enhanced crystallization at a higher temperature and the reduced total crystallinity. This reduced free motion is a result of the entrapment of a large percentage of polymer chains between clay particles that are not in contact with the remainder of the polymer phase. As the clay percentage is increased and a percolated network is formed, the large percentage of polymer entrapments results in altered crystallization kinetics.

Similar to the water vapor transmission rate, a mere 1 wt% clay loading has an evident influence on the crystallization of the composites. The most significant effects on crystallization behavior occur with the addition of a few weight percent of 30B, such that

the onset temperature of crystallization in the 1 wt% sample occurs 6.6˚C higher than neat PBAT. With the addition of 5 wt% 30B, the onset temperature is only 0.4˚C higher than that of the 1 wt% composite. Further, the increase in the onset temperature between the 5 and 10 wt% samples is only 3.72˚C. These results show that once the clay network has formed and most polymer chains are in direct contact with clay particles, additional clay loading does not have as large of an effect on polymer chain restructuring during crystallization.

To more closely examine the crystallization behavior near percolation, Figure 2.13 gives the onset crystallization temperatures as averaged from a minimum of three samples at each clay concentration. The cooling rate for these experiments was selected as 10˚C/minute to provide sharper crystallization peaks. Again, the onset temperature was increased by nearly 10˚C with the addition of 1 wt% clay. Further, the increase between the 3 wt% and 5 wt% composites is notably greater than the increase from 1 wt % and 3 wt% or 5 wt% and 7 wt%. This supports the findings that the percolated network develops near 4 wt%.

The other thermal analysis method that is of interest for both biodegradable and nonbiodegradable polymers alike is a study of the degradation behavior of the nanocomposites as clay levels are increased. Figures 2.14 and 2.15 show the TGA weight loss and derivative weight loss curves of approximately 12.0 mg of neat PBAT and 1-10 wt% 30B composites under 200 mL/min nitrogen and a heating rate of 10˚C/min. Table 2.2 summarizes the values calculated from the TGA curves in Figure

2.14 as well as the degradation behavior of pure Cloisite 30B which was dried under vacuum for 24 hours at 60˚C and kept in a desiccated environment until testing.

Assuming that the commutative property holds for TGA analysis, one can calculate the theoretical values of the weight loss of a composite during degradation based on the experimental weight losses measured of the pure components [58]. As a 10 mg sample of PBAT is heated through 550˚C, approximately 4 wt% (0.4 mg) of this sample should remain under these testing conditions. Correspondingly, a sample of clay can be expected to lose only approximately 30 wt% from thermal decomposition. If this 10 mg sample was instead composed of 90% PBAT and 10% 30B it could be calculated using the TGA results that 0.0405*(9.0 mg) + 0.7038*(1.0 mg) = 1.068 mg of the sample would remain. In this scenario, 10.7 wt% of the sample should remain after heating to 550˚C. The TGA results in Table 2.2 for the 10 wt% sample show that only 9.6% of the sample remained after testing. This indicates that the presence of clay may promote a slightly larger extent of PBAT chain degradation. This is further supported by the decrease in the onset and final temperatures associated with the degradation weight loss as the clay levels are increased in the samples. These results show that the degradation behavior of PBAT nanocomposites is similar to neat PBAT, and that the early onset degradation may in fact improve the flame retardancy of the composite through the premature formation of char and degradation products which inhibit flame propagation.

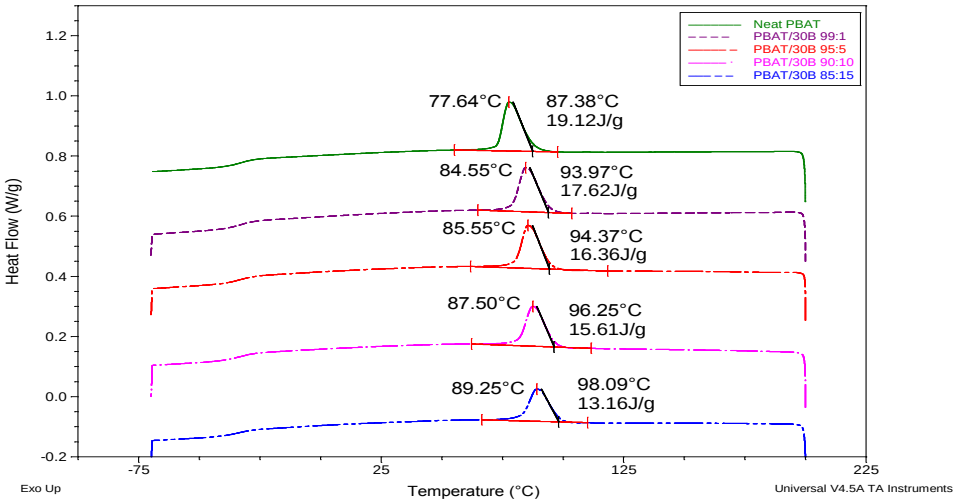


Figure 2.12. DSC Cooling Curves of PBAT Nanocomposites

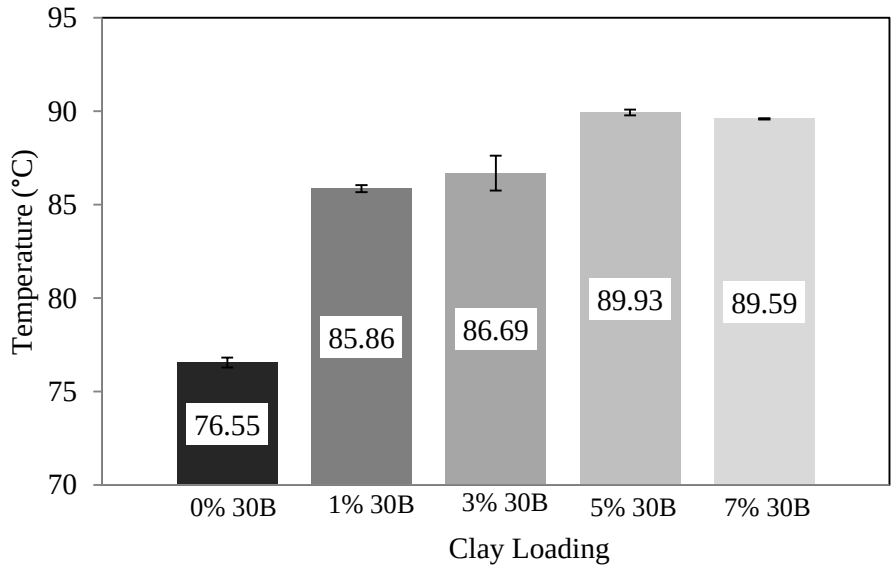


Figure 2.13. Onset Crystallization Temperature near Percolation

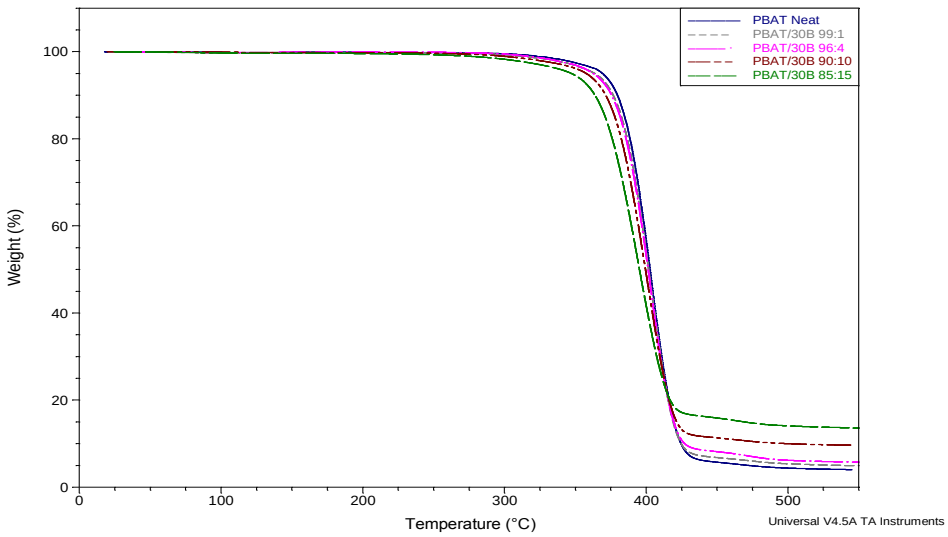


Figure 2.14. Thermogravimetric Analysis of PBAT Nanocomposites

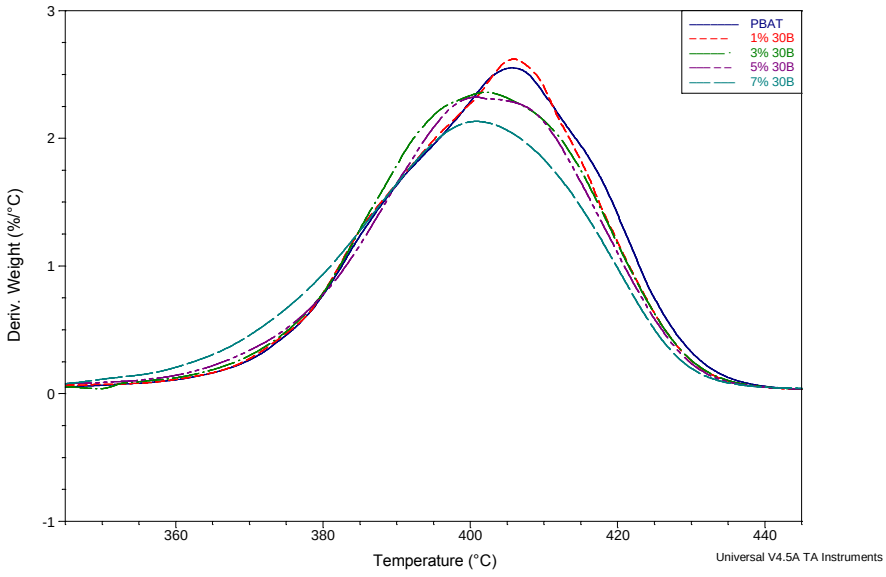


Figure 2.15. Derivative Weight Curve of PBAT Nanocomposites

Table 2.2. Summary Table of TGA Results

| PBAT:30B | $T_{deg,Onset}$ | $T_{max}$ | $T_{deg,Final}$ | Weight Loss (%) | 2% Weight Loss | Residue (%) T = 550 ˚C |
|---|---|---|---|---|---|---|
| 100:0 | 382.80 | 403.21 | 420.37 | 96.01 | 342.59 | 4.05 |
| 99:1 | 380.89 | 402.79 | 420.21 | 95.23 | 336.73 | 4.95 |
| 96:4 | 380.45 | 403.26 | 419.52 | 94.41 | 335.20 | 5.75 |
| 90:10 | 374.97 | 400.10 | 418.38 | 90.44 | 325.91 | 9.65 |
| 85:15 | 367.43 | 393.75 | 415.09 | 86.68 | 308.62 | 13.60 |
| 0:100 (1st Step) | 244.09 | 268.56 | 286.09 | 11.96 | 226.05 | 70.38 |
| 0:100 (2nd Step) | 286.09 | 399.40 | 432.12 | 18.43 | | |

## 2.7. CONCLUSIONS

Clay exfoliation was evidenced by XRD and an established nanoparticle network was made visible through TEM imaging of composites above the estimated percolation threshold. Water vapor transmission measurements further substantiated the development of a secondary clay structure above 2 wt% and no appreciable reduction in water vapor permeability when the clay concentration was increased to 5 wt%. The increase in the storage and loss modulus at low frequency indicates that the clay network forms above a clay loading of 3 wt% with a marked increase between 4 and 5 wt%. Through the plotting of the values of storage modulus at a chosen frequency for all prepared clay nanocomposites led to the identification of an experimental percolation threshold at approximately 3.8 wt%. The tensile modulus of all composites increased at the moderate expense of elongational properties. Interestingly, while the clay served as a

nucleating agent and crystallization was observed at higher temperatures during cooling, the overall crystallinity of the samples was considerably reduced at moderate to high clay loading levels.

# 3. FREE RADICAL MALEATION OF POLY(BUTYLENE ADIPATE-CO-TEREPHTHALATE) IN A SUPERCRITICAL CARBON DIOXIDE REACTION MEDIUM

## 3.1. INTRODUCTION

Graft copolymerization can enhance the properties of a polymer by adding specialty functional groups with varied hydrophilicity, polarity, and reactivity to a hydrophobic substrate. These slightly altered characteristics make graft copolymers useful in the compatibilization of polymer blends and filled polymer systems. Due to their limited commercial availability and narrowed processing ranges, altering the properties of biodegradable polymers through functional grafting helps to widen the applications in which they can be used. As an inexpensive and nontoxic substance with low critical properties, carbon dioxide can be used as a supercritical reaction medium for graft copolymerization and spent initiator extraction. This work discusses the grafting of a biodegradable polymer powder with a functional anhydride and the subsequent spectroscopic analysis of the grafted products.

## 3.2. FREE-RADICAL INITIATED POLYMER GRAFTING IN $SCCO_2$

Graft polymerization in a supercritical fluid provides a lowered solvent viscosity than solution and melt blending which provides an increased free radical efficiency with reduced cage effects. The diffusivity of a fluid above its critical point resembles that of a gas, and the fluid will readily penetrate and swell most polymers even if they do not fully dissolve. Thus, the effective surface area available for grafting is increased as compared to surface grafting processes such as radiation-induced functionalization. Carbon dioxide is commonly employed as a supercritical fluid for extraction processes due to its

comparatively low critical properties (a critical temperature of 31.1°C and a critical pressure of 7.39 MPa), and is therefore a sensible choice for the processing of temperature-sensitive biodegradable materials. Supercritical fluid processing of polymers exploits the plasticization of the amorphous sections of a semi-crystalline polymer, typically without altering the crystallinity of the final product significantly [39].

### 3.3. POLY(BUTYLENE ADIPATE-CO-TEREPHTHALATE)

Poly(butylene adipate-co-terephthalate) (PBAT) is a biodegradable thermoplastic with exceptionally good elongational properties, optical properties and wear-resistance. These characteristics make this aliphatic-aromatic copolyester the only compostable resin with properties similar to HDPE and it is correspondingly used in many single-use film applications in food packaging and agricultural and landscaping products. Figure 1.1 gives the structure of this random copolymer of butylene adipate and butylene terephthalate residues. By altering the ratio of butylene adipate and butylene terephthalate monomers, this copolymer can display a range of thermal and mechanical properties as well as biodegradation rates. As a semi-crystalline polymer, PBAT has been shown to swell significantly when exposed to $scCO_2$ [39]. This improves the rate of diffusion and impregnation of small molecules within the swollen PBAT matrix. While PBAT is commercially available, the limited literature on PBAT modification makes it a prime candidate for the supercritical graft copolymerization technique.

### 3.4. SUPERCRITICAL POLYMER GRAFTING REACTOR SYSTEM

Figure 3.1 depicts the supercritical grafting unit which consisted of a stainless steel, bolt-closure reactor with an internal volume of 300 cc. A heating jacket was fitted

around the reactor body for temperature control through a digital interface. The temperature was monitored by a Type-J thermocouple inserted in a thermowell through the reactor head and the pressure was monitored with an Omega pressure gauge. Carbon dioxide was fed from a booster pump to a storage vessel before being fed to the reactor system. The reactants were mechanically mixed and placed inside a stainless steel thimble, and a magnetically-driven impeller (MagneDrive®) was inserted in the thimble for homogenization of the reactor contents at a constant speed of 300 rpm. Tap water was used to cool the impeller and reactor system upon experiment completion. The reactor outlet line was directed through a 5-micron particle filter before entering an expansion drum.

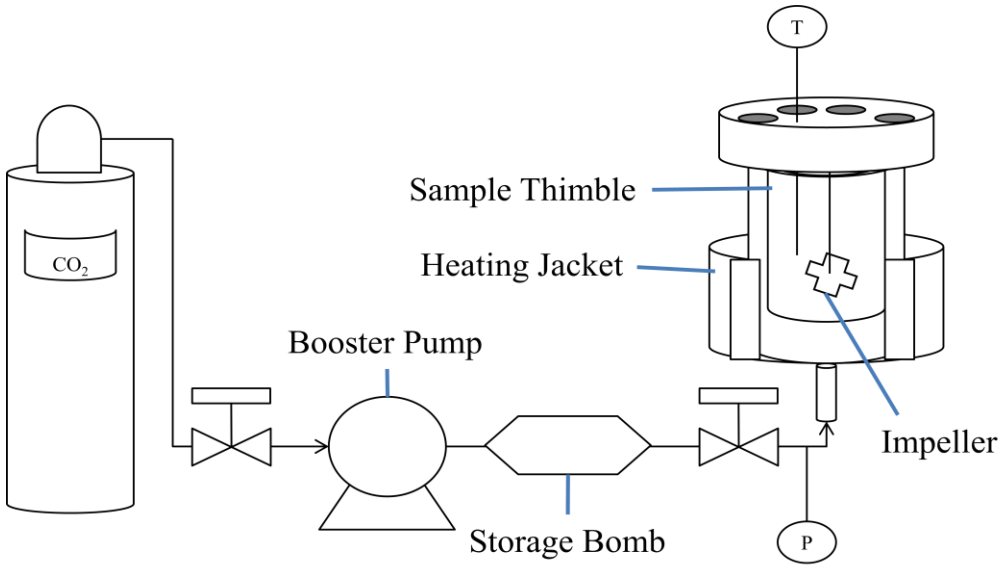


Figure 3.1. Supercritical Polymer Grafting Reactor Schematic

## 3.5. ANALYTICAL EQUIPMENT

Fourier Transorm InfraRed (FTIR) spectroscopy was performed with a Nicolet 6700 (ThermoFisher Scientific). Transmission experiments were carried out with 32 scans at a resolution of 2.0 from 4000-400 $cm^{-1}$ on melt pressed films or films cast from chloroform directly onto potassium bromide discs. The Smart iTR fixture was also used for attenuated total reflectance (ATR) spectroscopy by averaging 16 scans if the samples were highly absorbing in the region of interest. These scans were carried out from 4000-650 $cm^{-1}$ at a resolution of 4.0. The spectrometer was desiccated but not purged during use and thus the background water vapor and carbon dioxide were subtracted from all spectra before analysis. Proton ($^{1}H$) Nuclear Magnetic Resonance (NMR) spectroscopy was completed with a Varian INOVA 400 MHz FT/NMR in 5mm O.D. tubes at ambient temperature. The samples were dissolved at room temperature in deuterated chloroform (99.8 atom % D), and all spectra were corrected by the characteristic peaks of the chosen solvent (7.24 ppm for $^{1}H$ NMR and 77.0 ppm for $^{13}C$). Thermogravimetric analysis (TGA) was carried out with an SDT-Q600 (TA Instruments) on 15 mg samples under a purge flow rate of 200 mL/min nitrogen. All rheological properties were analyzed with a rotational rheometer, ARES-G2 (TA Instruments), in the parallel plate configuration. The stainless steel plates were 25 mm in diameter and all specimens were compression molded to a thickness of 1 mm.

## 3.6. SOURCE AND PREPARATION OF MATERIALS

**3.6.1. Materials.** PBAT was supplied by BASF under the registered name Ecoflex® F BX 7011, which has a MFR of 2.5 - 4.5 ml per 10 min and a density of 1.25 $g/cm^3$. Maleic anhydride (MA), 2,2'-azobisisobutyronitrile (AIBN), benzoyl peroxide

(BPO), methanol, tetrahydrofuran (THF), benzylamine (BA), n-pentane, and deuterated chloroform (99.8 %D) were purchased from Fisher Scientific. Ultra-high purity carbon dioxide and nitrogen (99.999%) was supplied by Praxair, Inc.

**3.6.2. Preparation of PBAT Powder.** The as-received polymer resin was first ground to a fine powder using a SPEX Sample Prep Freezer/Mill 6870. This milling process submerges a sample in a liquid nitrogen bath and then pulverizes it with a magnetically driven impactor according to the milling time programmed. Twenty grams of polymer pellets were placed in a large grinding vial and pre-cooled in a liquid nitrogen bath for five minutes prior to grinding. The vials were then put through four grinding cycles of five minutes each with three minutes of additional cooling between cycles. The polymer powder was then dried fully under vacuum at 50°C for 24 hours and kept in a desiccated environment until use.

**3.6.3. Supercritical Graft Copolymerization.** At the beginning of each experiment, the system was pressurized to 500 psi and then vented slowly three times to remove oxygen and water vapor from the vessel. The system was then taken to a median pressure between ambient and the experimental pressure and the heating system was turned on. The desired temperature and pressure was reached through the slow addition of carbon dioxide and heat. Once the set point density was reached, the reactor temperature and pressure were recorded every five minutes to ensure that the fluid density remained constant throughout the experiment. Upon completion, the reactor was cooled and vented slowly over a 60 minute period to avoid polymer foaming.

**3.6.4. Reactive Extrusion of PBAT-g-MA.** The properties and processability of PBAT-g-MA which was prepared through reactive extrusion was also compared to PBAT grafted via $scCO_2$. The extruded PBAT-g-MA was processed in a Brabender parallel twin screw extruder with three heating zones that were maintained at 145, 145, and 149˚C. PBAT pellets was dried at 50˚C for 24 hours prior to extrusion and premixed with maleic anhydride powder (pulverized from briquettes) and dicumyl peroxide. From literature, the optimal monomer and initiator loading was determined to be 2.5 wt% maleic anhydride and 0.5% peroxide [31, 35, 59, 60].

**3.6.5. Soxhlet Extraction.** The high sensitivity analysis that is essential to the verification and quantification of low level polymer grafting necessitates a more rigorous removal of spent initiator and excess monomer. In order to provide a product for direct spectroscopic analysis, Soxhlet extraction with methanol was employed. This method is widely-used in purification and removal of excess reactants [61]. The extraction technique, as pictured in Figure 3.2, utilizes a cellulosic thimble in a glass extraction system that produces a reflux of 200 mL of methanol at its boiling point. Approximately 10-20 grams of sample is placed in a 32 mm thimble and refluxed for 24 hours before removal. While Soxhlet extraction effectively removes all residual monomer and initiator, the reaction of the grafted maleic anhydride functionality with the methanol solvent opens the anhydride ring, producing an ester and an acid group. The product must then be dried under vacuum for at least 24 hours to re-close the anhydride ring before further spectroscopic analysis.

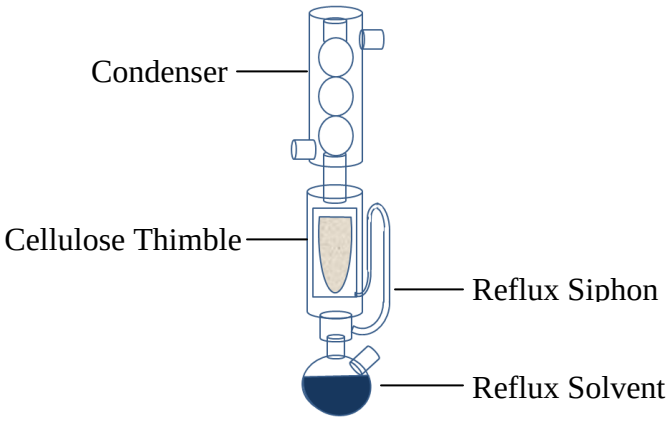


Figure 3.2. Soxhlet Extraction Apparatus

**3.6.6. Amination of Maleated PBAT.** The grafting reaction of MA is easily controlled, as steric hindrance only permits a single MA monomer to attach to the polymer backbone and subsequent polymerization of MA does not occur as can be seen in Figure 3.3. This benefit of the maleation reaction, however, makes identification and verification of the grafted moiety difficult through spectroscopic methods, particularly at grafting levels below 5 percent. To improve the detection process, the anhydride group can be reacted with an amine with a more easily detected long alkyl chain or benzyl group [63, 64]. The maleic anhydride attachment is easily controlled and the reaction of the anhydride functionality with an amine is rapid and well-studied. This amination is also often employed in order to affix additional functional groups or bioactive components on polymeric substrates. In one particular example, poly(lactic acid) was grafted with maleic anhydride and then further reacted with ethylenediamine, producing a polymer substrate with improved cytocompatibility which was attributed to the neutralization of the degradation products by the ethylenediamine [22].

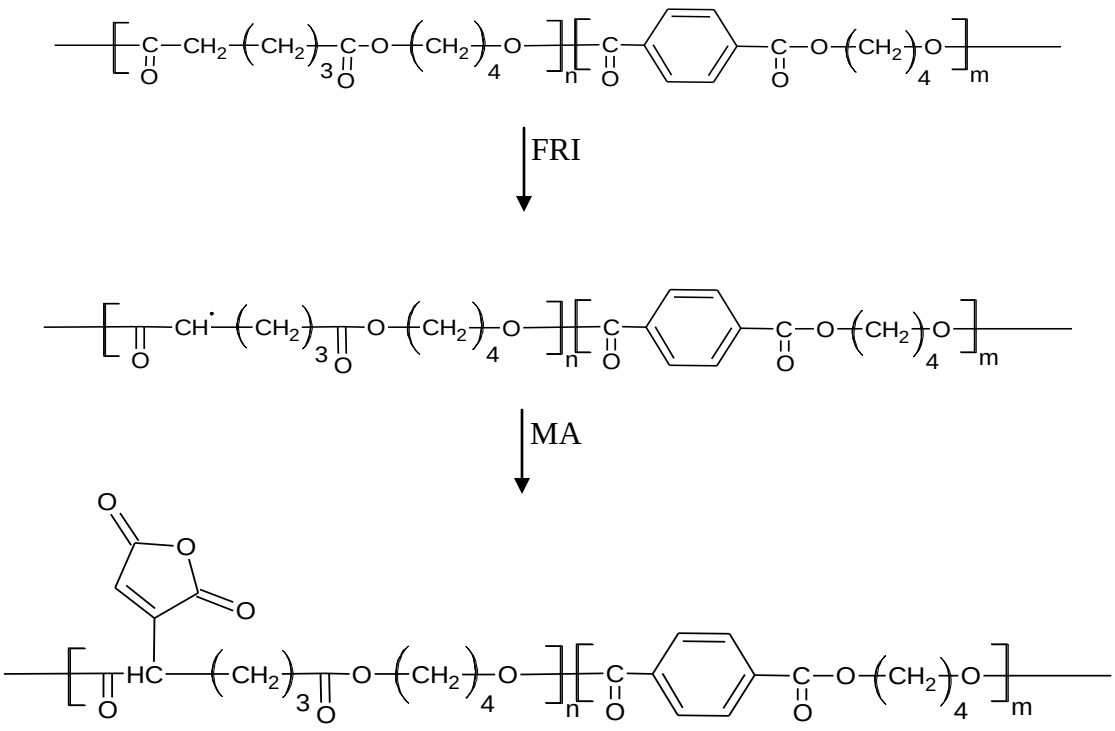


Figure 3.3. PBAT Maleation Reaction Mechanism

For this work, the PBAT-g-MA was further reacted with benzylamine (BA) in order to increase the hydrogen signals associated with the grafted group by a factor of five. One-gram samples were dissolved in 75 mL of THF and an excess of BA was added dropwise to the solution. The solution was agitated and maintained at room temperature, as the reaction between maleic anhydride an amine has been found to be reversible at elevated temperatures [64]. While below 40°C this amination is expected to occur rapidly, the reaction was allowed to proceed for two hours to ensure completion before the product was precipitated in pentane. The aminated product was then dried at ambient conditions to constant weight and then dissolved in THF and precipitated in pentane two additional times to remove any excess BA.

## 3.7. EXPERIMENTAL CONDITIONS

**3.7.1. Solvent Density.** As the reaction medium temperature is varied, the solvent density must be controlled to provide a supercritical fluid system that has comparable diffusivity in the PBAT powder, solvent strength, and dielectric constant for each experiment. The equation of state chosen to estimate the solvent density of the carbon dioxide phase was the Peng-Robinson equation, as it is typically the most accurate relationship for estimating the state variables of nonpolar liquid and supercritical fluids and mixtures.

The solvent density was estimated for all target experimental conditions by an iterative calculation process, where Z is calculated by:

$$Z = 1 + \beta - q\beta \frac{(Z - \beta)}{(Z + \varepsilon\beta)(Z + \sigma\beta)}$$

where the constants ε and σ are defined as: $\varepsilon = 1 - \sqrt{2}$ and $\sigma = 1 + \sqrt{2}$ for the Peng-Robinson Equation and the values of q and β are calculated from:

$$\beta = \Omega \frac{P_r}{T_r} \quad and \quad q = \frac{\psi\alpha(T_r)}{\Omega T_r}$$

$$\alpha_{PR} = [1 = \ 0.37464 + 1.54226\omega - 0.26992\omega^2 \quad 1 - T_r^{\frac{1}{2}} \ ]^2$$

where $T_r$ and $P_r$ are the reduced temperature and pressure of the system as compared to the critical values for carbon dioxide and $\omega$ is the acentric factor of carbon dioxide. A value for Z is first set to 1.0 and then the remainder of the calculations are carried at the experimental reaction temperature and pressure to calculate a new Z value. This process is repeated until the returned Z value is the same as the initial input value and then the molar volume and solvent density can be calculated from:

$$V\left[\frac{cm^3}{mol}\right] = \frac{ZRT}{P} \quad and \quad \rho\left[\frac{g}{cm^3}\right] = \frac{MW_{CO_2}}{V}$$

Using this iteration, the solvent density was estimated for all experimental conditions in order to determine target pressure and temperature settings. The targeted solvent density for all experiments was 300 kg/m$^3$ as suggested in previous a sc$CO_2$ graft copolymerization publication [41]. To ensure that these conditions were met within the constant volume batch system, the pressure must be increased when the temperature is increased for a particular experiment.

During system start-up, $CO_2$ was charged at room temperature to the reactor and then heated to the experiment set point. To increase the operating pressure, additional $CO_2$ could slowly be added to the batch system from the storage bomb which was held at 3000 psig. As the monomer and initiator are both readily soluble in sc$CO_2$, the reactor contents could not be vented once supercritical conditions were met. Thus, some variance in density was possible due to the difficulty in controlling the amount of $CO_2$ initially charged to the reactor through the inlet valve. For all experiments discussed in this work, the calculated solvent density from the experimental data fell in the range of 295-329 kg/m$^3$.

**3.7.2. Temperature Selection.** The effectiveness of free radical initiated grafting reactions is primarily determined by the thermal effects on the initiator throughout the experiment. The temperature is thus the main parameter to control in order to maximize the level of grafting and minimize the time required for the reaction to come to completion.

In order for the grafting reaction to be effective, the operating temperature must be above both the critical temperature of $CO_2$ (31.1°C) and the $T_g$ of the polymer and also

below the onset melting temperature of the polymer phase. Figure 3.4 shows the second heating curve of neat PBAT powder at a heating rate of 10°C/min under a nitrogen flow rate of 50 mL/min. This curve gives a $T_g$ approximately -30°C and $T_m$ of 126.84°C. Due to the random copolymer backbone, the maximum melting rate of PBAT is achieved near 125°C but the melting endotherm is relatively wide and the first deviation from the baseline can be seen at temperatures as low as 90°C.

The operating temperature range is further specified by the chosen free radical initiator activity and the temperature at which its degradation rate is optimal for promoting grafting within a reaction time that minimizes degradation of the base polymer. Two free radical initiators were selected in order to study the grafting reaction at various temperatures while maintaining the same solvent density. Benzoyl peroxide (BPO) is a commonly used free radical initiator in polymer grafting which undergoes one bond scission during thermal degradation and the rate of BPO decomposition has been shown to increase as much as 10% in a $scCO_2$ medium as compared to decomposition kinetics in n-heptane [32]. Highly active above 80°C, only 10% of BPO remains after three hours of exposure to temperatures above 90°C [41].

AIBN (2,2'-azobisisobutyronitrile) was also used in the experiments carried out at lower temperatures due to its higher level of activity below 80°C, as compared to BPO. While the decomposition mechanism of AIBN involves the breaking of two bonds, the dissociation has been shown to occur at nearly the same rate in various solvents. The lower dielectric constant of $scCO_2$ may slow the degradation slightly, but the initiator efficiency is increased due to the low viscosity of scCO2 which reduces the cage effects

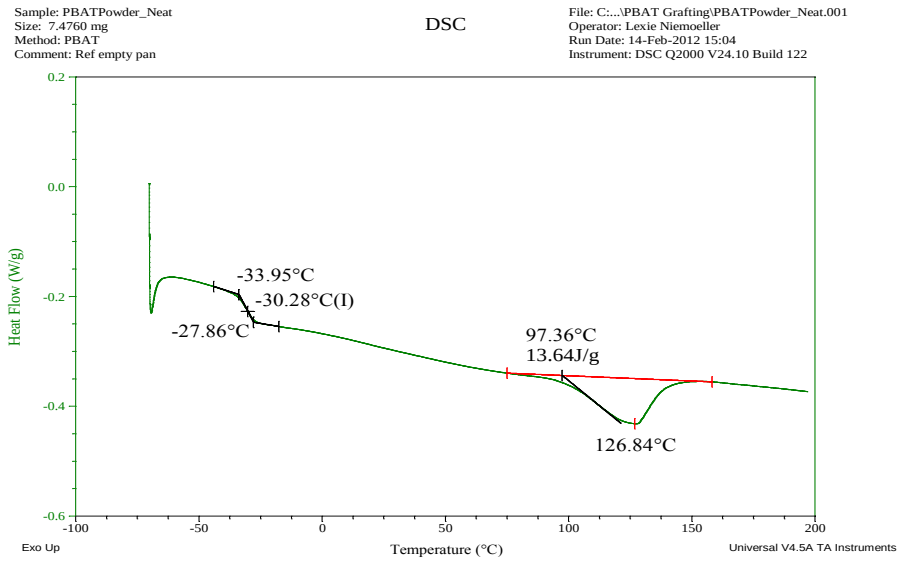


Figure 3.4. DSC Heating Curve of Neat PBAT for the Selection of Process Temperature

which commonly affect free radical reactions [65]. AIBN was found to be active at temperatures above 50˚C with a calculated activation energy of 134.6 kJ/mol in $scCO_2$, which is on the order of its activation energy in other solvents (120-140 kJ/mol) [66].

**3.7.3. Monomer and Free Radical Concentration.** The graft level achieved through free-radical maleation has been found to be directly related to the amount of radicals present in the system and correspondingly the level of macroradical sites created [67]. It has also been reported that as the maleic anhydride amount increased, the graft level increased but only to a certain point. Above 6 MA phr (parts per hundred polymer units) the graft level was found to decrease. Through $^{13}C$ NMR and GPC analysis of PP-g-MA, it was also found that extremely high levels of MA can lead to increased beta scission of the polypropylene backbone and a reduced molecular weight during grafting

[68, 69]. Based on these previous studies, the selected condition for all experiments was 10 wt% MA and 2.5 wt% free-radical initiator.

**3.7.4. Reaction Time.** To minimize the detrimental effects on the biodegradable polymer, the target reaction time was chosen as 180 minutes. One experiment was examined at a moderate temperature of 75˚C but a reaction time of 240 minutes to yield comparable free radial initiator activity.

**3.7.5. Experimental Matrix.** Table 3.1 lists the selected experimental conditions which were examined in this study. Three experiments were conducted with AIBN and three were conducted with BPO, at varying temperatures and pressures resulting in a density near 300 kg/m$^3$.

Table 3.1. Selected Experimental Conditions

| Experiment Name | Free Radical Initator | Temperature (°C) | Solvent Density (kg/m$^3$) | Run Time (min) |
|---|---|---|---|---|
| PBAT - 01 | AIBN | 70.2 | 310.9 | 180 |
| PBAT - 02 | AIBN | 75.6 | 298.2 | 240 |
| PBAT - 03 | AIBN | 85.5 | 295.2 | 180 |
| PBAT - 04 | BPO | 82.0 | 320.9 | 180 |
| PBAT - 05 | BPO | 84.6 | 329.0 | 180 |
| PBAT - 06 | BPO | 90.0 | 287.2 | 180 |

## 3.8. PRODUCT CHARACTERIZATION

**3.8.1. Effects of Grafting Method on Polymer Processability.** One major driving force behind the use of $scCO_2$ for polymer grafting, is the mild conditions employed during the reaction. Reactive extrusion, alternatively employs high heat and

shear rates while simultaneously mixing free radicals into the polymer phase. Under these processing conditions, the molecular weight distribution (MWD) of the macromolecule can be significantly altered [67-69]. If the radicals formed on the polymer backbone lead to cross-linking, the average molecular weight, viscosity and gel-content of the product is increased. Alternatively, unstable radicals produced at the polymer backbone may lead to chain scission and a reduction in molecular weight and viscosity. Thus, when dealing with free radicals it is imperative to investigate the relationship between processing conditions and final processability of the graft copolymer.

In Figure 3.5, the complex viscosity of PBAT-g-MA produced via reactive extrusion is plotted against frequency. This dynamic frequency sweep was conducted at 5% strain and 140˚C. As compared to the neat PBAT pellets extruded without MA or BPO, the complex viscosity is markedly lower. This indicates that the presence of the

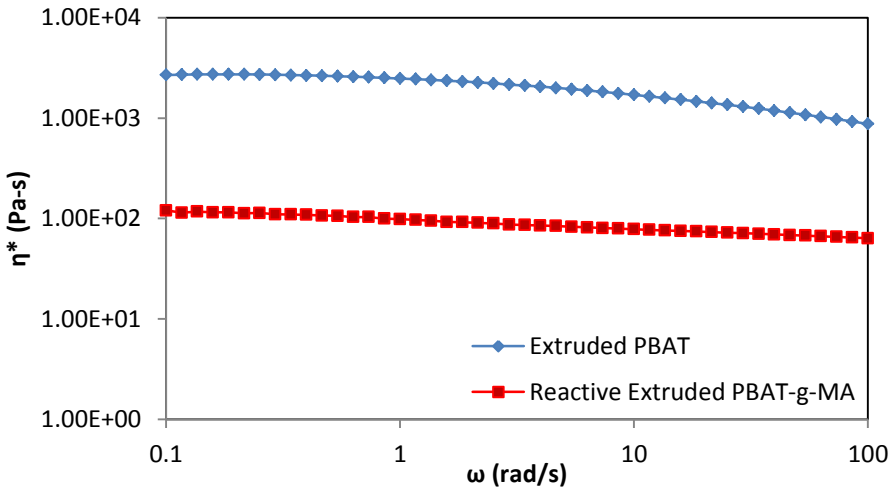


Figure 3.5. Complex Viscosity of Extruded PBAT and PBAT-g-MA

monomer and initiator under elevated temperature and shear causes significant chain scission in PBAT. This finding is interesting, given that the long branched structure of PBAT is often compared to that of HDPE which generally demonstrates cross-linking and an elevated viscosity during reactive extrusion [23].

**3.8.2. Removal of Spent Initiator and Excess Monomer.** While the Soxhlet extraction method used subsequent to the grafting reaction is a well-practiced method, it must be verified that the spent initiator and ungrafted monomer have been fully removed before further analysis. Figure 3.6 is the FTIR-ATR spectra of a PBAT-g-MA sample which was processed via $scCO_2$. The two peaks at approximately 1775 and 1850 $cm^{-1}$ correspond to the excess un-grafted anhydride functionalities that remain in the samples. After Soxhlet extraction, the FTIR-ATR curve no longer shows these anhydride peaks, however, this does not indicate that the maleation of PBAT has not occurred. The grafting of maleic anhydride only attaches a single monomer to a free radical site, thus it is extremely difficult to detect a graft level of 1-5%.

Figure 3.7 gives the TGA curve and derivative of the weight loss curve to help clearly indicate where the weight loss transitions occur. The first weight transition curve for the PBAT-g-MA sample prior to Soxhlet extraction accounts for the excess MA and FRI that is present in the grafted sample. Given that the initial concentration of the monomer and initiator was 10% and 2.5%, respectively, the 10.77% weight loss between 80-127.7˚C is reasonable. Other than the MA which was successfully grafted to PBAT, it can be assumed that the remainder of the monomer and initiator were lost through the venting process of reactor, as these small molecules are soluble in $scCO_2$.

**3.8.3. Identification of Grafted Moieties.** Spectroscopy serves as the most effective way to observe a small molecule which has been affixed to the backbone of a polymer. This is particularly true for graft copolymerization, where the graft level is expected to be below 10%.

**3.8.3.1. FTIR spectroscopy.** As shown Figure 3.6, it is extremely difficult to view the attached MA functionality directly through FTIR spectroscopy of PBAT-g-MA. This is due to the small size of this particular grafted moiety, the typically low level of grafting achieved, and the presence of a highly absorbing carbonyl bond in the PBAT backbone. This peak at approximately 1720 $cm^{-1}$ can overlap where the succinyl anhydride group of grafted MA would appear in the FTIR spectrum. Even at high grafting levels, only a weak shoulder can be viewed at the side of this peak.

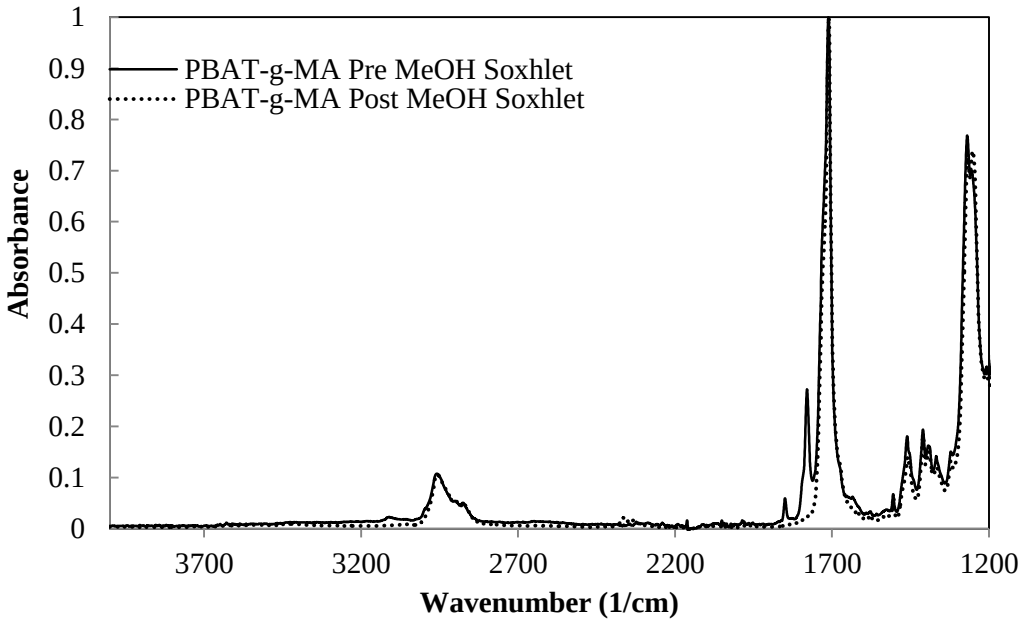


Figure 3.6. FTIR-ATR of PBAT-02 before and after Methanol Soxhlet Extraction

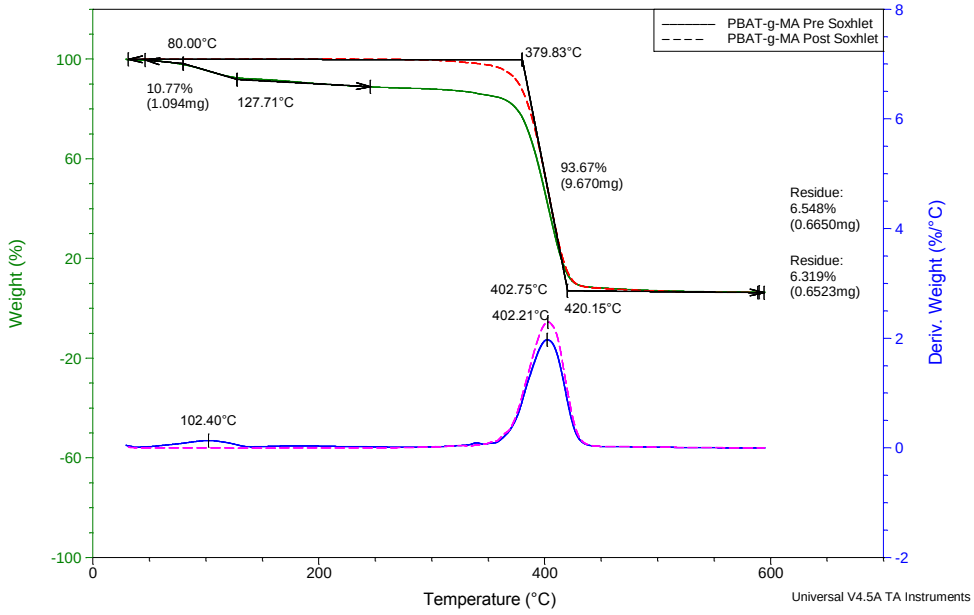


Figure 3.7. Thermogravimetric Analysis of PBAT-g-MA before and after Soxhlet Extraction

Upon the amination of the grafted samples, the detection of successful grafting can be carried out much more readily. Figures 3.8 and 3.9 show the emergence of the characteristic benzylamine peak near 700 $cm^{-1}$. This peak also appears as a shoulder to a larger peak present in neat PBAT and thus the graft can be observed but not easily quantified in through this spectroscopic method.

**3.8.3.2. $^{1}$H NMR spectroscopy.** Proton NMR served as the most sensitive method for graft observation and graft level determination. Figure 3.10 shows the $^{1}$H NMR spectrum for neat PBAT, which has been corrected by the characteristic peak of the chloroform solvent which appears at 7.24. Figures 3.11-15 are the PBAT-g-MA samples which were aminated with BA prior to NMR analysis. The benzylamine

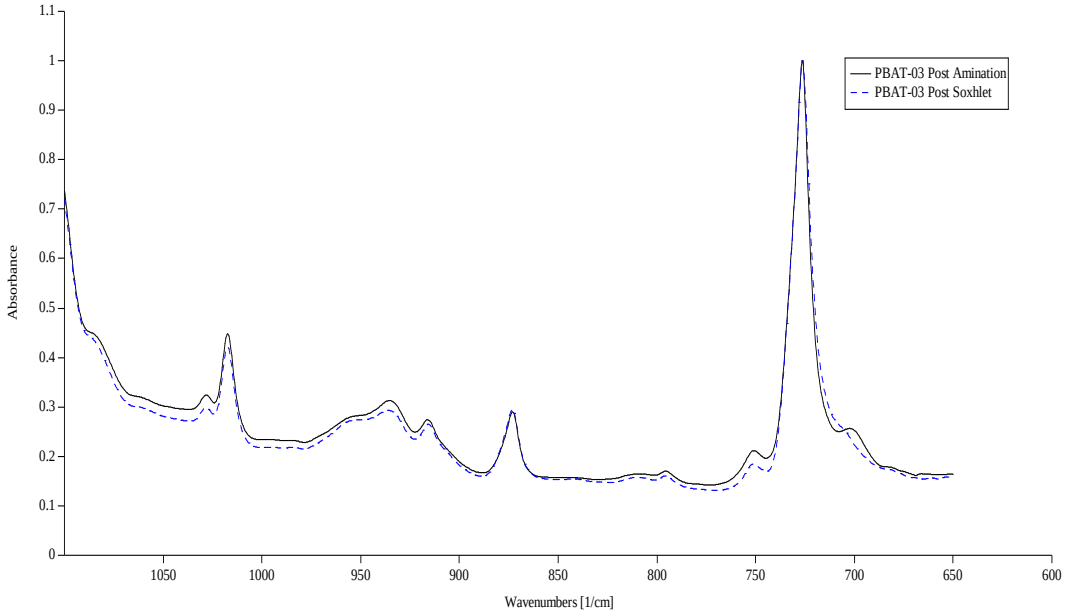


Figure 3.8. Characteristic Benzylamine Peak in FTIR-ATR Spectra of PBAT-03

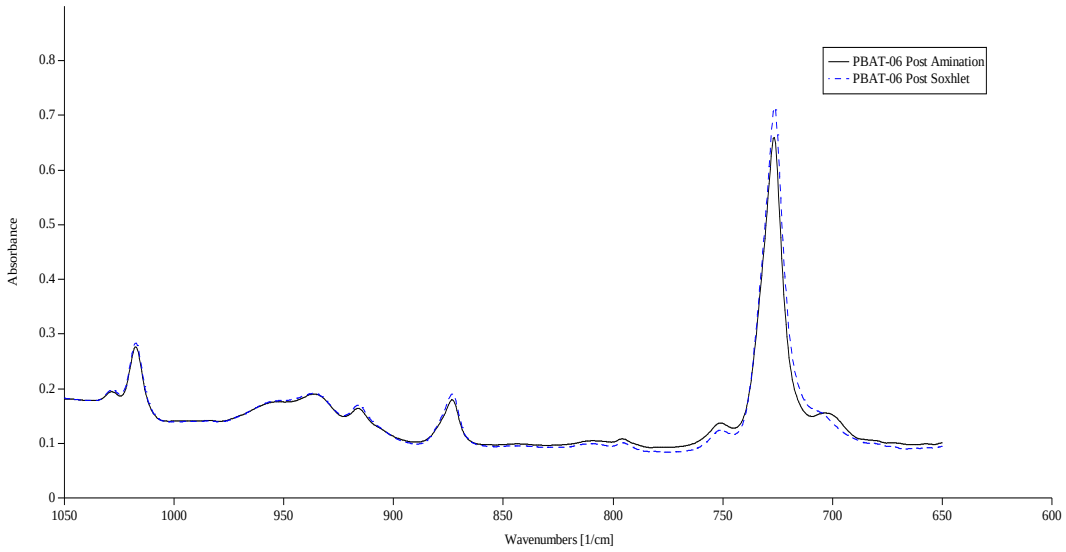


Figure 3.9. Characteristic Benzylamine Peak in FTIR-ATR Spectra of PBAT-06

peak appears at 7.3 ppm and can be assigned to the hydrogen located on the benzyl ring. By integrating these curves and comparing them to the characteristic peaks of PBAT, the graft levels can be estimated and are summarized in Table 3.2. This integration was performed with SpinWorks software after manual phase and baseline corrections.

Grafting was detected for five of the selected experiment conditions with the graft level ranging between 1.16 – 1.63%. The one experiment which did not show an appreciable BA peak was PBAT-01 which was the experiment conducted at the lowest temperature of 70˚C. While this temperature is within the range of AIBN activity, the grafting reaction did not proceed. Upon a slight increase in temperature to 75.6˚C and an increase in reaction time to 240 minutes, the PBAT-02 sample displayed a BA peak that correlated to a graft level of approximately 1.29%. A further increase in temperature to 85.5˚C resulted in the highest graft level measured of 1.63%. While this result would indicate that the graft level increases with temperature, the samples grafted with BPO displayed the opposite trend with the maximum graft level for BPO (1.53%) occurring at a temperature of 82.0 and a density of 321 $kg/m^3$ and the lowest graft level was measured at the highest experimental temperature of 90˚C. This is an unexpected result, as the activation energies for radical dissociation, addition, and termination are predicted to be higher at elevated temperatures [34]. One explanation for this result could be that higher local concentrations of the reactants at lower temperatures could raise grafting efficiency and mitigate radical dissociation throughout the duration of the experiment.

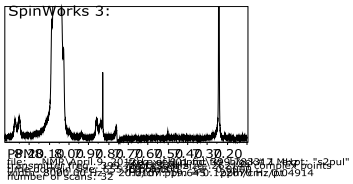


Figure 3.10. $^{1}$H NMR Spectrum of Neat PBAT

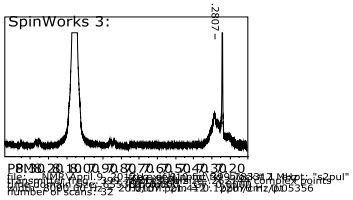


Figure 3.11. $^{1}$H-NMR of PBAT-02 Post-amination with BA

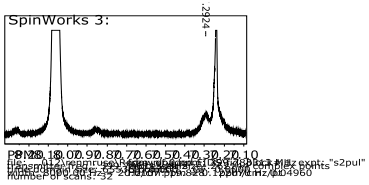


Figure 3.12. $^{1}$H NMR of PBAT-03 Post-amination with BA

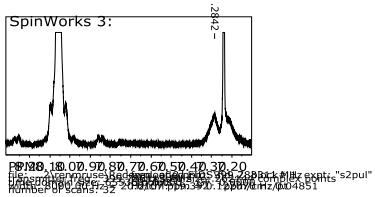


Figure 3.13. $^{1}$H NMR of PBAT-04 Post-amination with BA

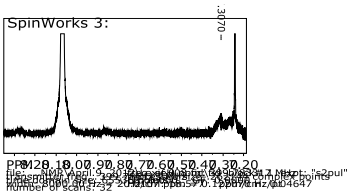


Figure 3.14. $^{1}$H NMR of PBAT-05 Post-amination with BA

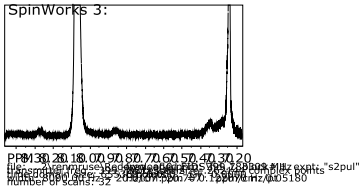


Figure 3.15. $^{1}$H NMR of PBAT-06 Post-amination with BA

Table 3.2. Graft Level of Selected Experiments

| Experiment Name | Free Radical Initiator | Temperature (°C) | Solvent Density ($kg/m^3$) | Graft (%) |
|---|---|---|---|---|
| PBAT – 01 | AIBN | 70 | 310.9 | 0.00 |
| PBAT– 02 | AIBN | 75.6 | 298.2 | 1.29 |
| PBAT – 03 | AIBN | 85.5 | 295.2 | 1.63 |
| PBAT – 04 | BPO | 82.0 | 320.9 | 1.53 |
| PBAT – 05 | BPO | 84.6 | 329.0 | 1.47 |
| PBAT – 06 | BPO | 90.0 | 287.2 | 1.16 |

## 3.9. CONCLUSIONS

The maleation of biodegradable PBAT was demonstrated in a supercritical carbon dioxide medium. Two free radical initiators were used to compare the grafting efficiency of peroxide an azo-initiated graft copolymerization in a supercritical fluid. To aid in the detection of the grafted functionality, benzylamine was affixed to the anhydride ring through an amination reaction in a THF cosolvent. The characteristic peaks of benzylamine were observed with both FTIR and $^1H$ NMR spectroscopy. The achieved graft level estimation was calculated to be between 1.16-1.63% through integration of the peaks in the NMR spectra; and from these calculated graft levels, it was determined that this technique is most effective within the temperature ranges of 75-85°C for AIBN initiation and 80-90°C for BPO initiation. All experiments outside of these temperature ranges produced no detectable benzylamine peaks with spectroscopic analysis. For the evaluation of rheological properties, PBAT-g-MA was also prepared via reactive extrusion with dicumyl peroxide. The reactive extruded samples exhibited a lowered melt viscosity which can be attributed to polymer chain scission and a reduced average

molecular weight of the product, due to elevated temperature and high shear melt processing in the presence of free radicals. These results demonstrate that the supercritical graft copolymerization method is a viable alternative to polymer grafting in the melt or solution phase with either an azo-type or a peroxide free radical initiator.

# 4. UTILIZATION OF PBAT MALEATED IN SUPERCRITICAL CARBON DIOXIDE AS A COMPATIBLIZER FOR PBAT NANOCOMPOSITES

## 4.1. INTRODUCTION

The limited number of commercially-available biodegradable polymer resins has generated great interest in the area of the modification and the compatibilization of biodegradable polymer blends and composites. Graft copolymerization can be used to impart new functionalities and alter the properties of polymer matrices, ultimately improving the properties of composite products through a reduction in the interfacial tension. Through the maleation of PBAT in a supercritical carbon dioxide medium, a compatibilizer was produced for PBAT/clay nanocomoposites. The effects of the addition of 5% PBAT-g-MA to PBAT nanocomposites were then studied through rheology, permeation, and thermal analysis, and the dispersion and exfoliation state of the nanoclay phase was characterized through x-ray diffraction and electron microscopy.

**4.1.1. Supercritical Carbon Dioxide Grafting.** For compostable materials such as poly(butylene adipate-co-terephthalate) (PBAT), the method utilized for polymer grafting must be optimized for temperature-sensitive materials and must also retain degradability in the final product. Supercritical carbon dioxide grafting provides an organic solvent-free reaction environment at temperatures significantly lower than the most widely used alternative method, reactive extrusion. The grafting technique employed for the production of PBAT-g-MA was carried out with 5 wt% maleic anhydride and 2.5% free radical initiator at a carbon dioxide density of 300 kg/m$^3$ for 180 minutes.

**4.1.2. Nanocomposite Percolation and Compatibilization.** Nanoscale fillers have been shown to have significant effects on the thermal, mechanical, and rheological behavior of polymer composites. The high aspect ratio of nanoscale materials provides for increased surface contact, thus the reduction of aggregates and enhancement of filler dispersion are the key issues in the optimization of nanocomposite properties. Graft copolymers are often used in compatibilizing hydrophobic polymer chains with natural fillers to improve filler dispersion. For layered silicate composites, compatibilizers like maleated polymers improve tactoid dispersion and platelet exfoliation. This has been reported to occur through a combination of surface interactions leading to clay layer removal as well as polymer chain diffusion into the gallery spacing resulting in platelet delamination [42, 43]. The altered kinetics of these mechanisms with the addition of a polar anhydride functionality can increase clay exfoliation further, causing a percolated clay network at a lower clay loading than in a noncompatibilized polymer matrix. The previously reported percolation threshold of PBAT-Cloisite 30B nanocomposites is 3.88 wt%, thus the compatibilized samples developed in this work are expected to exhibit a percolated structure below this clay concentration.

## 4.2. MATERIALS AND METHOD

**4.2.1. Materials.** PBAT was supplied by BASF under the name Ecoflex® F BX 7011, which has a MFR of 2.5 - 4.5 ml per 10 minutes and a density of 1.25 g/cm$^3$. The surface area of the PBAT pellets was increased prior to supercritical grafting by cryogenic grinding as described in Section 3.6.2. The layered silicate was provided by Southern Clay under the product name Cloisite® 30B. The organic modification of this particular MMT clay is a quarternary ammonium with a bulky tallow group. The PBAT

powder, pellets and clay were dried under vacuum at 50˚C for a minimum of 24 hours before processing. Maleic anhydride, 2,2'-azobisisobutyronitrile, benzoyl peroxide, dicumyl peroxide, methanol, tetrahydrofuran, benzylamine, n-pentane, and deuterated chloroform (99.8 %D) were purchased from Fisher Scientific. Ultra-high purity carbon dioxide and nitrogen (99.999%) were supplied by Praxair, Inc.

**4.2.2. Processing Equipment.** The supercritical grafting reaction was performed in the stainless steel bolt-closure reactor depicted in Figure 3.1. The melt compounding of the nanocomposites and the reactive extrusion experiments were carried out with the twin screw extruder as described in Section 2.4. A Carver press was used to prepare 0.24 mm thick films for permeation analysis and 1 mm sheets for rheological and tensile testing.

**4.2.3. Reactive Extrusion.** For comparison of the effectiveness of the proposed compatiblization technique, a common solvent-free grafting method was also carried out. Simultaneous reactive extrusion and clay compounding was demonstrated by premixing the PBAT pellets and nanoclay with MA and dicumyl peroxide (DCP) before extrusion. The selected composition of the monomer and initiator were 2.5 wt% and 0.5 wt%, reportedly the optimal conditions for grafting with minimal side reactions such as chain scission and cross-linking [30-33].

**4.2.4. Analytical Equipment.** X-ray diffraction patterns were captured using a PANalytical X'Pert PRO MRD with a copper anode, a wavelength of 1.54 angstroms, and a divergence slit of 0.05 mm. The diffractograms were captures from $1^\circ < 2\Theta < 10^\circ$. Images of the clay structure in the PBAT matrix were captured with a JEOL JEM-1400F

transmission electron microscope. To produce specimens thin enough for TEM imaging, the extrudate pellets were first sectioned with an ultramicrotome.

The rheological response of the prepared nanocomposites was studied on an ARES-G2 rheometer (TA Instruments) in the 25 mm diameter parallel plate configuration. Specimens were cut from 76 x 76 x 1 mm molded sheets into 25 mm diameter circles. All tests were conducted at 145˚C and a strain of 3%, and the samples were compressed to a gap of 0.95 mm to ensure consistent plate contact and sample volume between tests.

The water vapor transmission rate through the prepared nanocomposite films was studied according to ASTM-E96/E96M-10. Films (0.24 +/- 0.007 mm thickness) were secured with silicone wax to glass containers which were filled with an 8 mesh desiccant and then sealed. The testing chamber was maintained at 27°C and 75% humidity throughout the testing period, with a constant air velocity provided by a fan. The weight of each sample was taken every 12 hours over a four-day period and adjusted relative to the weight change of a prepared "dummy" sample without desiccant. The water vapor transmission rate was then calculated as the average of the corrected weight change of three samples of each clay loading studied.

Crystallization studies were performed with a DSC-Q2000 (TA Instruments) on 10 mg samples at a heating and cooling rate of 10˚C/min. Thermogravimetric analysis (TGA) was conducted with an SDT-Q600 (TA Instruments) with heating rate of 10˚C/min and 15 mg samples were used for all degradation studies. A nitrogen purge

was used at a flow rate of 50 and 200 mL/min for the DSC and TGA analyses, respectively.

Tensile testing of the prepared composites was performed with a universal testing machine (Instron model 4469) according to ASTM D638. A type IV dumbbell specimen and a crosshead speed of 10 mm/s was used for the Instron analysis at ambient conditions.

## 4.3. RESULTS AND DISCUSSION

**4.3.1. TEM Imaging.** Transmission electron microscopy offers a facile way to examine composites at the nano-scale and observe slight changes in clay structure. Figure 4.1 gives multiple magnifications of a 3% clay nanocomposite with and without the addition of 5 wt% PBAT-g-MA compatibilizer. The top set of images (the non-compatibilized samples) show a high percentage of clay particles (the dark areas in the images) present in multi-layer tactoids and a larger distance between neighboring clay particles. The light areas in the TEM images correlate to the PBAT matrix, and the high percentage of white space in the non-compatibilized samples signify that there is limited interaction between the polymer and clay phases.

The images taken of the compatibilized samples show a much higher level of clay exfoliation, with numerous individual clay platelets separated from the clay tactoids. These exfoliated layers help to reduce the interparticle distance and increase the interactions between neighboring clay particles, helping to develop a secondary clay network within the composite. This exfoliation can be attributed to the grafted anhydride functionality which has been shown to improve the interfacial interactions between the PBAT chains and the surface of organically-modified MMT. In the lower images of

Figure 4.1, the separation of individual platelets from a stack of clay can be seen at all three magnifications. It has been hypothesized that the bi-functional MA encourages clay platelet separation by two methods: (1) surface interactions which "peel" each layer from the clay tactoid and (2) favorable interactions between MA and the organic modifications within the clay gallery space induce clay layer expansion and subsequent exfoliation [48]. It is not clear from these images alone which of these methods is valid, but the enhanced dispersion and exfoliation are evident.

Images were also captured of the prepared 5 wt% 30B composites and are collected in Figure 4.2. The top two images represent the nanocomposites that were compatibilized with 5 wt% PBAT-g-MA from the scCO2 grafting method and the bottom two images correspond to a sample that was reactive extruded according to the method described above. There are very few individual clay lamellae in the reactive extruded samples and the visible clay tactoids are markedly larger than in the $scCO_2$ compatibilized nanocomposites.

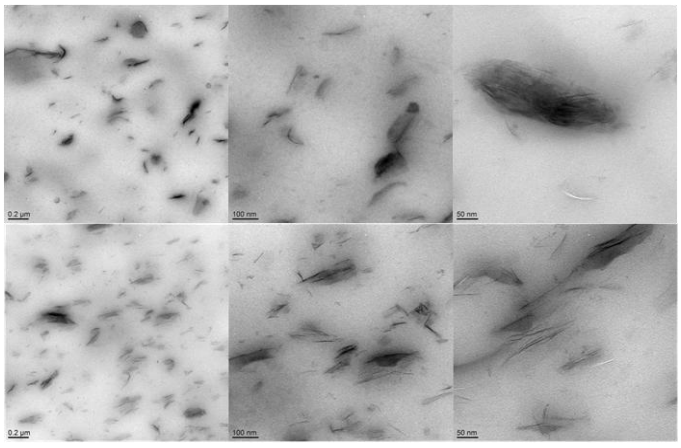


Figure 4.1. TEM Images of 3 wt% 30B PBAT Nanocomposites
Top: No compatibilizer Bottom: 5% PBAT-g-MA
Magnification Scale (from Left to Right): 200 nm, 100 nm, 50 nm

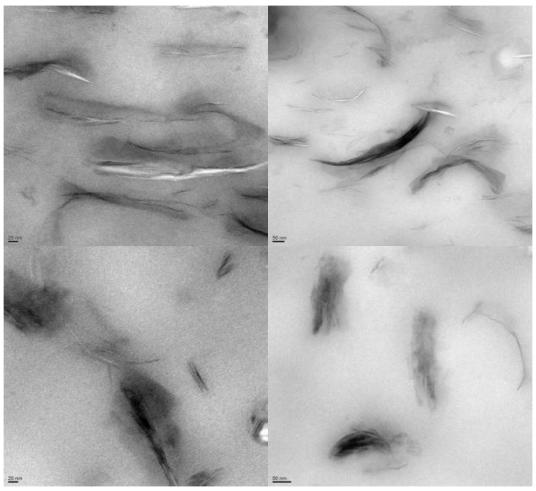

Figure 4.2. TEM Images of 5 wt% 30B PBAT Nanocomposites
Top: Compatibilized with 5 wt% PBAT-g-MA
Bottom: Reactive Extruded with 2.5 wt% MA and 0.5 wt% DCP
Magnification Scale: 20 nm (Left) and 50 nm (Right)

**4.3.2. X-Ray Diffraction.** The study of x-ray diffraction between clay layers provides a more holistic interpretation of the clay exfoliation state than individual TEM images of thin slices of a clay nanocomposite sample. A peak in an x-ray diffractogram indicates that an ordered structure exists in the sample, and for layered silicates the distance between clay layers can be calculated from Bragg's Law:

$$n\lambda = 2d\sin\Theta$$

where n is an integer, $\lambda$ is the wavelength of the incident x-ray, d is the distance between successive clay layers, and $\Theta$ is the angle between the x-ray and the diffracted ray. Cloisite 30B has a gallery spacing of 18.5 angstroms which leads to a $d_{001}$ peak at $\Theta$ = 2.39° or at $2\Theta$ = 4.78° for an incident x-ray of 0.154 nm.

In Figure 4.3, the x-ray diffraction patterns are shown for pure Cloisite 30B and for two PBAT nanocomposites with 3% Cloisite 30B, one non-compatibilized and one

compatibilized with 5 wt% PBAT-g-MA. The characteristic peak of the clay appears at approximately $2\Theta = 4.8°$ as Bragg's Law predicts. The compounding of clay with PBAT causes this peak to reduce in height as the clay tactoids are exfoliated and broken apart under high shear in the extruder. The shift of the peak to the left (lower values of $2\Theta$) also indicates that the clay platelets that remain in stacks have been separated slightly. The non-compatibilized 3 wt% clay composite shows a broad peak at approximately $2\Theta = 2.245°$ which correlates to an expanded gallery spacing of 39.3 angstroms. Most interestingly, the x-ray diffractogram of the compatibilized sample contains no measurable diffraction peak. While this result alone is not sufficient to confirm full clay exfoliation, the disappearance of this diffraction peak is often attributed to the existence of primarily clay monolayers in the sample [48-50].

A similar set of x-ray diffractograms is given for both non-compatibilized and compatibilized PBAT nanocomposites at a clay loading of 5 wt% in Figure 4.4. Without the addition of a compatibilizer, the clay peak is present at $2\Theta = 2.345°$ or a clay layer separation of 37.6 angstroms. The compatibilized sample still shows a clay diffraction peak at $2\Theta = 2.45°$ or a gallery spacing of 36.0 angstroms, but it is significantly narrowed and reduced in height.

**4.3.3. Water Vapor Transmission.** As determined in previous work, the higher the clay loading, the more resistant the film is to water vapor permeation due to the increased tortuosity of the path a molecule must take in order to pass through the film. The clay particles are predominantly oriented perpendicular to the direction of diffusion, and the high aspect ratio of the tactoids and platelets greatly improve the barrier properties of polymer films at loadings less than 10 wt%.

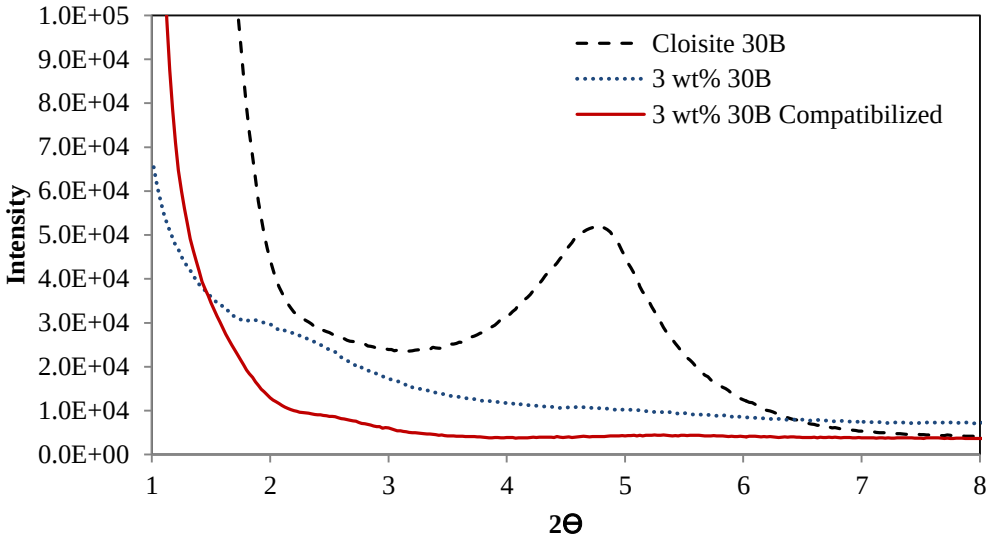


Figure 4.3. X-Ray Diffractogram of PBAT Nanocomposites with 3% 30B

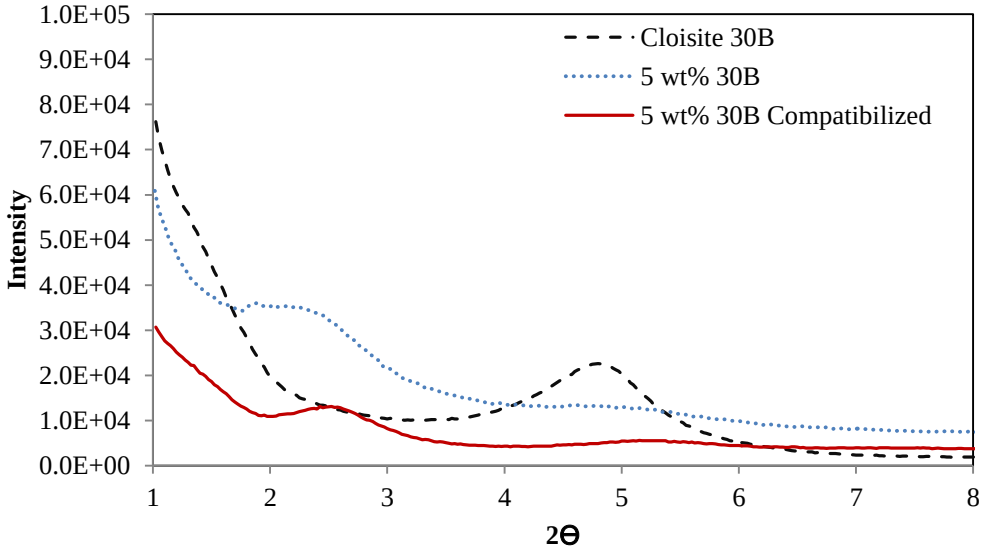


Figure 4.4. X-Ray Diffractogram of PBAT Nanocomposites with 5% 30B

Figure 4.5 shows the average water vapor transmission measured through three melt pressed PBAT films at clay loadings of 3 and 5 weight percent. The transmission rate is notably reduced upon incorporation of PBAT-g-MA in the films in both clay loadings examined. The transmission rate through the 3 wt% 30B nanocomposite film is reduced by 25.5% to 29.9 g/m$^2$/day and the 5 wt% nanocomposite film water permeability was reduced 21.2% to 26.1 g/m$^2$/day. Further, the compatibilized 3 wt% film provides better resistance to water vapor permeation than the 5 wt% film without compatibilizer. This is expected to be caused by the increased level of exfoliation in the compatibilized samples as observed through both TEM and XRD analyses. The reduced number of aggregates that can lead to perforations in the film, and the larger number of individual clay lamellae result in films with reduced permeability. While the presence of MA on the surface of a polymer substrate can alter its polarity and hydrophilicity, the graft level is low enough that this does not have an appreciable deleterious effect on the

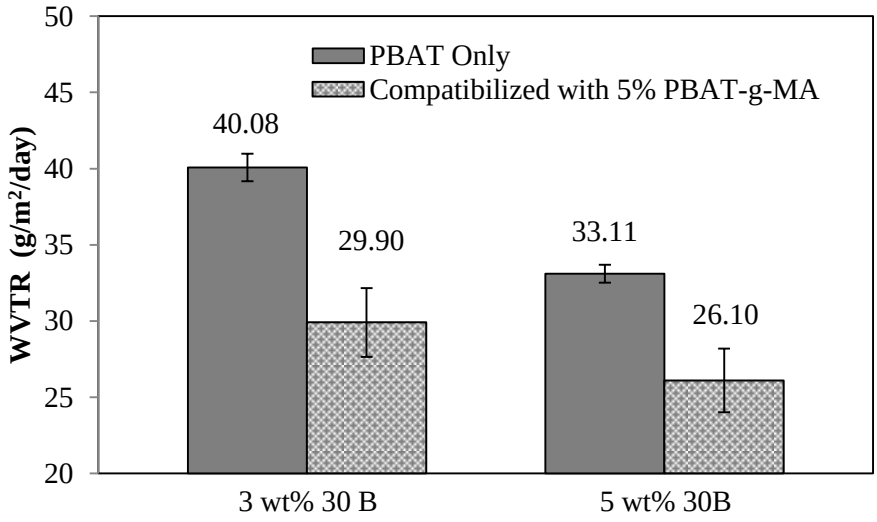


Figure 4.5. Water Vapor Transmission through Compatibilized PBAT Nanocomposites

water vapor absorption of the films and the overall effect is an improvement in the barrier properties of PBAT. Interestingly, the difference between the permeation of the non-compatibilized samples is larger than that between the compatbilized film samples. This may indicate that the percolation threshold of the compatibilized samples is below 3 wt% instead of falling within the 3-5 wt% range.

**4.3.4. Melt Rheology.** The detection of an ordered structure at the nanometer level within a polymer matrix can be challenging but is often possible with microscopy and x-ray patterning. To observe slight changes in the structure of clay particles, a more sensitive testing method such as dynamic oscillatory shear rheology is required. When a small strain is applied at a low frequency to a polymer nanocomposite in the melt phase, it will respond as a pseudo-solid if the clay layers have formed a secondary network. Thus, melt rheology can be used to determine the effectiveness of a graft copolymer in enhancing clay exfoliation and lowering the percolation threshold of a particular composite.

In Figure 4.6, the storage modulus (G') of PBAT nanocomposites are compared over a frequency range of 0.1-100 rad/s at a strain rate of 3% and a temperature of 145°C. As mentioned in previous work, PBAT nanocomposites at a clay loading of 3 wt% and below do not show a significant low frequency plateau in G'. Above the estimated percolation threshold of 3.88 wt%, the storage modulus is less dependent on frequency and the nanocomposite displays the more solid-like viscoelastic response under low frequency shear which is visible in the G' values of the 4 wt% composite in Figure 4.6. The compatibilized 3 wt% 30B sample shows a median response between the 3 and 4 wt% clay loading level, which is indicative of a higher level of clay exfoliation and a

percolation threshold which has shifted below 3 wt%. The frictional forces between clay particles are the cause of this response and are only detected when a high level of dispersion and exfoliation result in a large percentage of clay particles which interact directly with at least one neighboring particle. As the frequency is increased, this nanostructure is destroyed and G' for all samples approach that of neat PBAT.

A nearly identical trend can be seen in the complex viscosity (η*) of the same nanocomposites in Figure 4.7. The viscosity of the non-compatibilized 3 wt% 30B composite is essentially identical to that of neat extruded PBAT. The compatibilizer elevates the complex viscosity in the terminal region, which is characteristic of a pseudo-solid polymer material that undergoes shear-thinning as the frequency increases.

The efficacy of the PBAT-g-MA as a compatibilizer can even be seen at a clay loading level as low as 1 wt% 30B in Figure 4.8. While the low frequency G' plateau is slight and was only detectable by reducing the frequency to 0.05 rad/s, this finding signifies that a network began to develop with the addition of only 1 wt% clay and 5 wt% graft copolymer. The detection of this small change in the viscoelastic response of this composite is only possible through with the use of a rheometer with a transducer that is separated from the motor responsible for the oscillatory strain, which results in separate stress and strain measurements and improved accuracy. Thus, melt rheology was the chosen method to analyze the efficacy of the two free radical initiators used during the supercritical grafting reaction.

Both peroxide- and azo-type free radical initiators have been shown to successfully graft MA to the PBAT backbone in $scCO_2$ at approximately the same graft

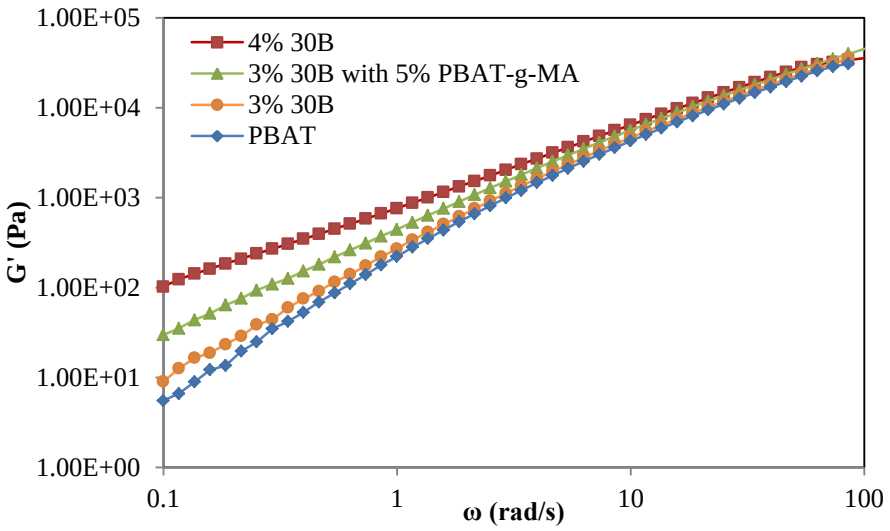


Figure 4.6. Low Frequency Plateau in G' of Compatibilized PBAT Nanocomposites

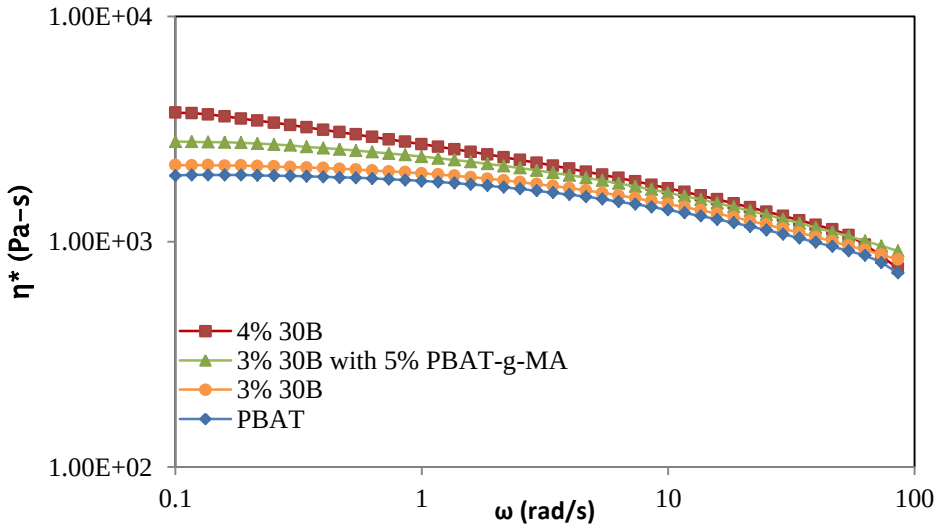


Figure 4.7. Complex Viscosity of Compatibilized PBAT Nanocomposites

level, as determined through $^{1}H$ NMR spectroscopy. Dynamic frequency melt rheology can also be used to comparatively study the compatibilization achieved with the two samples of PBAT-g-MA, one copolymerized with AIBN and one with BPO. Figure 4.9 shows the G' of a 3 wt% clay nanocomposite as well as the compatibilized samples from these two grafting methods. The low frequency increase in G' is nearly identical for the two compatibilized nanocomposites, further indicating that the graft level achieved with AIBN and BPO and the efficacy of the resultant PBAT-g-MA products in improving clay exfoliation are analogous. These findings help to validate the use of either type of initiator and widen the operating temperature window for $scCO_2$ graft copolymerization. For biodegradable polymer grafting, it is particularly important to explore the effectiveness of various free radical initiators and determine which provides optimal grafting efficiency at an ideal processing temperature.

Figures 4.10 and 4.11 exhibit the storage modulus and complex viscosity values of compatibilized and non-compatibilized 5 wt% 30B samples. These results are analogous to the altered low frequency response of the 3 wt% composites, with the compatibilized 5 wt% sample displaying an even higher level of frequency independence. The relative slope of the G' curve for the non-compatibilized 5 wt% sample is 0.62 as compared to neat PBAT, and for the compatibilized sample the relative slope is reduced to 0.40. With PBAT-g-MA, the G' and $\eta^*$ values of the 5 wt% 30B nanocomposite approach the frequency independence that is seen in true solids.

For further justification of this compatibilization method, the viscoelastic response of neat PBAT was compared to that of a nanocomposite obtained through

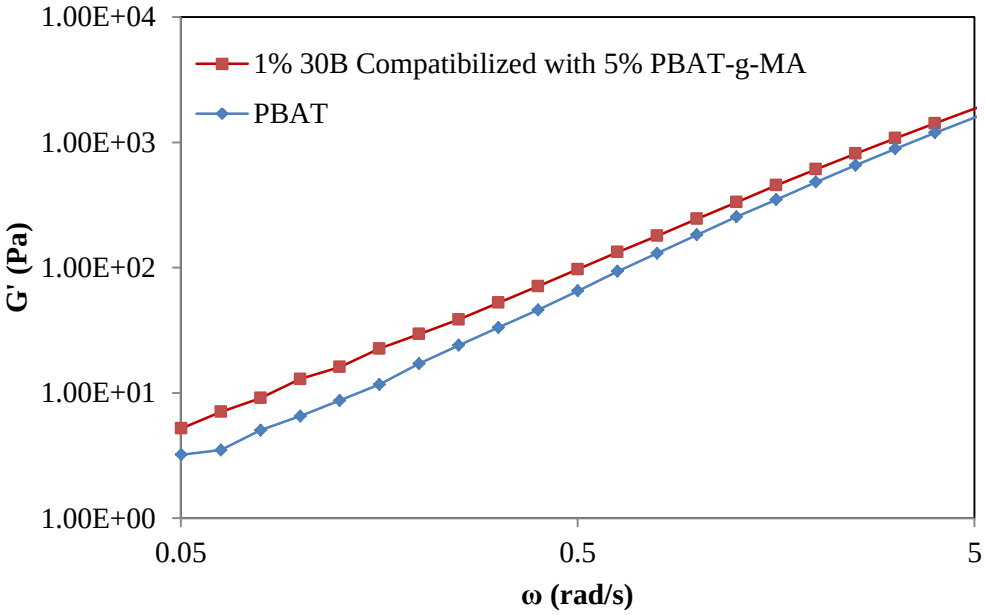


Figure 4.8. Ultra Low Frequency G' Plateau

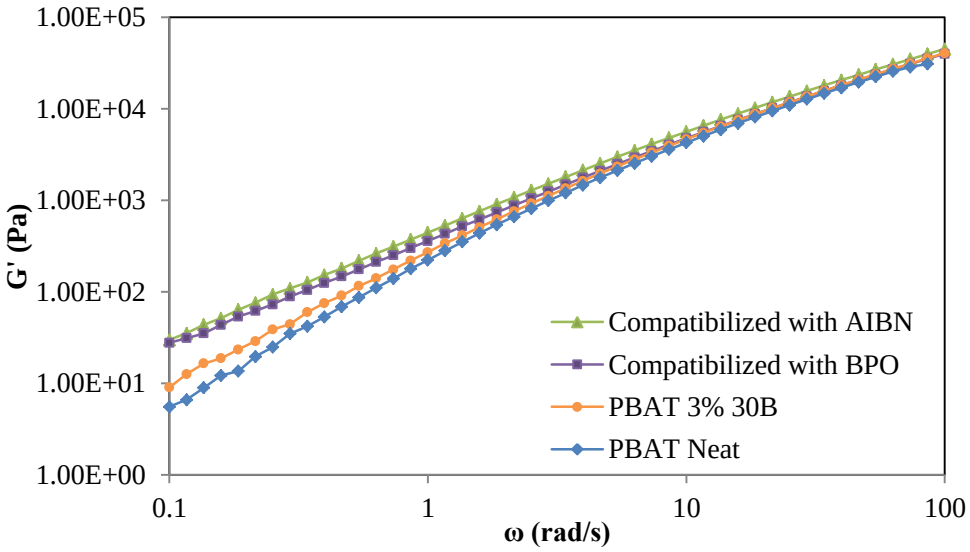


Figure 4.9. Comparative Study of Two Free Radical Initiators in PBAT-g-MA Compatibilization

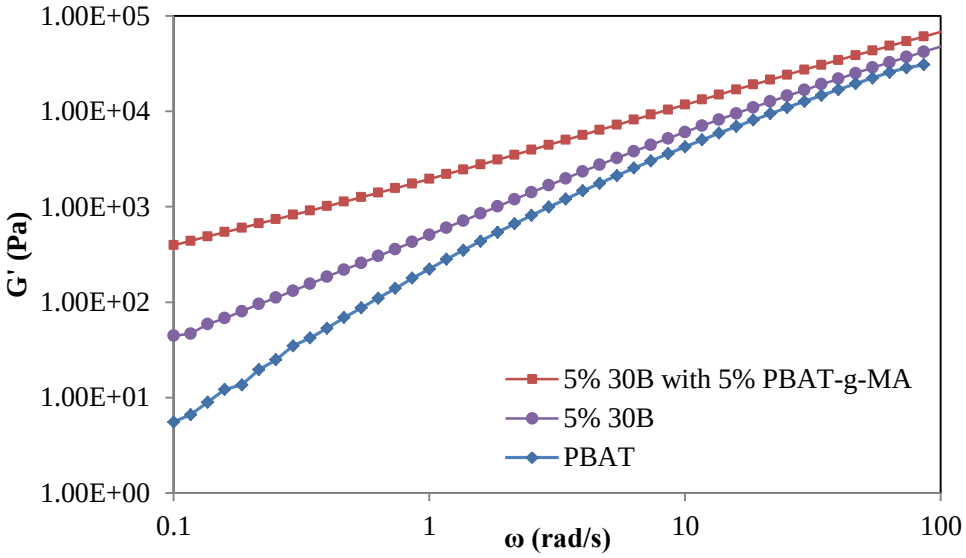


Figure 4.10. Storage Modulus of Compatibilized Composite with 5% Nanoclay

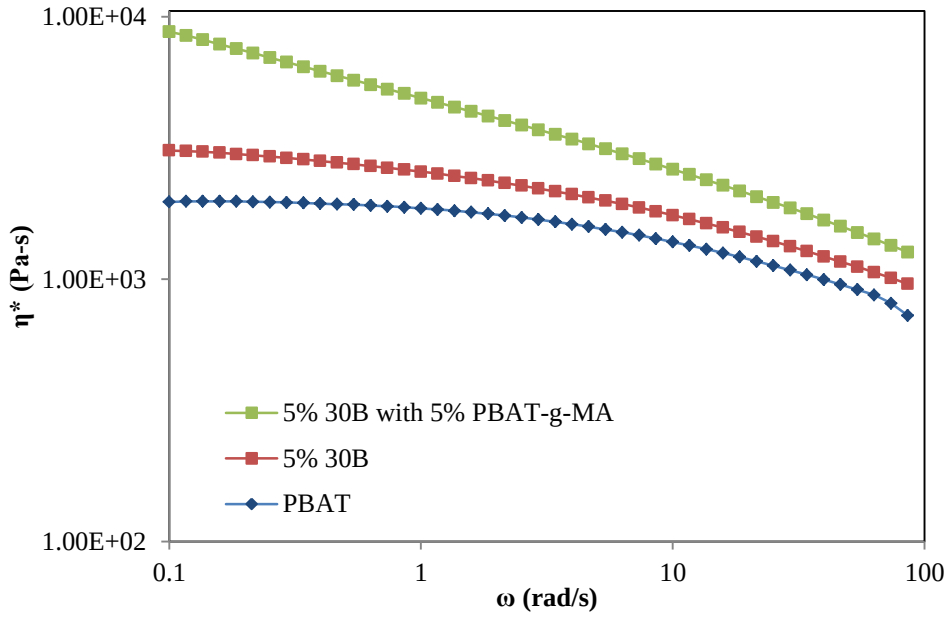


Figure 4.11. Complex Viscosity of Compatibilized 5 wt% PBAT Nanocomposite

reactive extrusion. While the one-step process of simultaneous grafting and clay compounding is simple to conduct, the exposure of a biodegradable melt to free radicals under high shear results in a clear reduction in product viscosity as seen in Figure 4.12. The melt incorporation of 5 wt% clay typically raises the complex viscosity of PBAT, but in the presence of a peroxide and maleic anhydride the resultant viscosity of the nanocomposite is lowered. This is assumed to be due to extensive main chain scission and widening of the molecular weight distribution. In some applications, the utilization of peroxides during extrusion is ideal for molecular weight control but this methodology is difficult to control for biodegradable polymers. The isolation of free radical exposure to the milder reaction conditions provided by $scCO_2$ results in less polymer degradation and a product with a more consistent molecular weight.

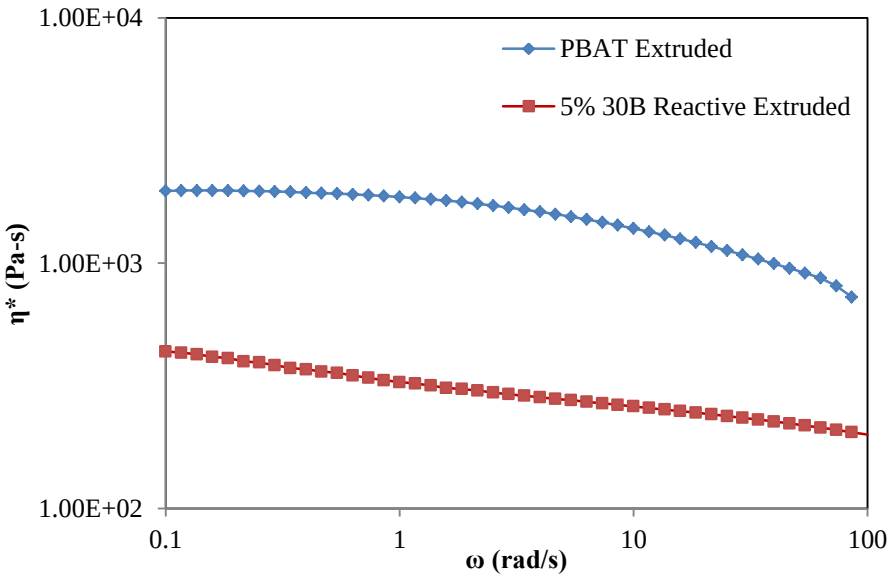


Figure 4.12. Complex Viscosity Reduction with Reactive Processing

**4.3.5. Thermal Analysis.** The exfoliation and dispersion state of a layered silicate nanocomposite can be indirectly observed by determining the temperature at which the material undergoes a thermal transition such as crystallization or degradation. A small amount of compatibilization which leads to enhanced clay exfoliation can be detected through a study of altered crystallization and/or degradation kinetics.

Differential scanning calorimetry (DSC) can be used to determine if a process has altered the structure of the polymer matrix of a nanocomposite by measureing a shift in the glass transition ($T_g$) temperature. As is often the case with $scCO_2$ processing, the $T_g$ is unchanged for all clay contents analyzed. Table 4.1 lists the $T_g$ values averaged from three samples of each compatiblization experiment and the temperatures do not vary from the $T_g$ of neat PBAT by more than +/- 0.5°C. Thus, while the supercritical grafting process temporarily increases the free volume of the material and plasticizes the PBAT polymer chains, the utilization of PBAT-g-MA that has been supercritically processed does not have an effect on the glass transition of the nanocomposite.

Table 4.1. Glass Transition Temperature of Compatibilized PBAT Nanocomposites

| Sample | $T_g$ (°C) | +/- |
|---|---|---|
| PBAT | 30.41 | 0.66 |
| 1% 30B | 30.34 | 0.80 |
| 1% 30B Compatibilized | 30.09 | 0.71 |
| 3% 30B | 30.12 | 0.29 |
| 3% 30B Compatibilized | 30.64 | 0.46 |
| 5% 30B | 31.09 | 0.34 |
| 5% 30B Compatibilized | 30.57 | 0.08 |
| 7% 30B | 30.96 | 0.57 |
| 7% 30B Compatibilized | 30.99 | 0.58 |

The cooling curves of PBAT as well as two PBAT nanocomposites with 3 wt% 30B are given in Figure 4.13. Neat PBAT exhibits a sharp crystallization peak with a maximum crystallization rate at 71.92°C and onset crystallization occurring at 76.26°C. The 3 wt% clay composite begins to crystallize at 87.07°C and the maximum crystallization occurs at 78.31°C. Upon compatibilization with 5% PBAT-g-MA, this crystallization peak shifts to even higher temperatures and crystal growth begins at nearly 90°C. A similar trend is shown in Figure 4.14 for a compatibilized sample with 7 wt% clay, where the onset and maximum crystallization appear at 92.46 and 83.47°C, respectively.

In comparing Figures 4.13 and 4.14, it can be seen that the compatibilized 5 wt% clay sample exhibits onset crystallization at higher temperatures than the non-compatibilized sample with 7 wt% clay content. This is a key example of the effects of compatibilization leading to improved disruption of the layered clay structure and enhanced interactions between the polymer chains and the clay surface. As the tactoids are separated to single and multi-layer platelets, additional clay surface is exposed which serve as nucleating sites for crystal growth upon cooling. There is a more significant effect on the onset of crystallization upon the PBAT-g-MA compatibilizer than by adding an additional 2 wt% nanoclay. This effect is summarized in Figure 4.15, where the average temperature of maximum crystallization rate is given for a minimum of 3 samples at each clay loading level, both with and without PBAT-g-MA compatibilizer. It is also worth noting that while the crystallization temperature of the non-compatibilized samples increases with increased clay loading, this effect is minimized above the percolation threshold of the composite which was determined from previous work to be

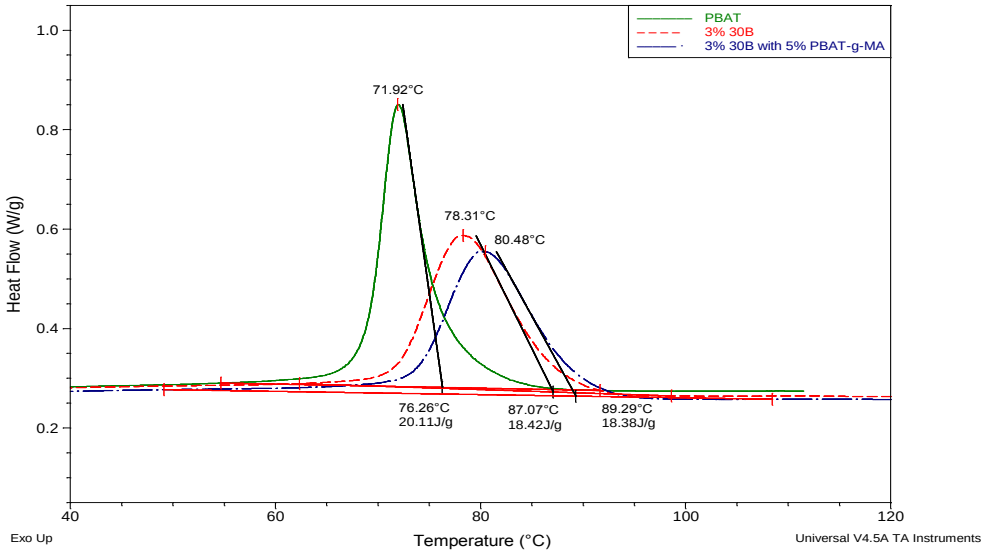


Figure 4.13. Increased Crystallization Temperature in Compatibilized Nanocomposite with 3 wt% Cloisite 30B

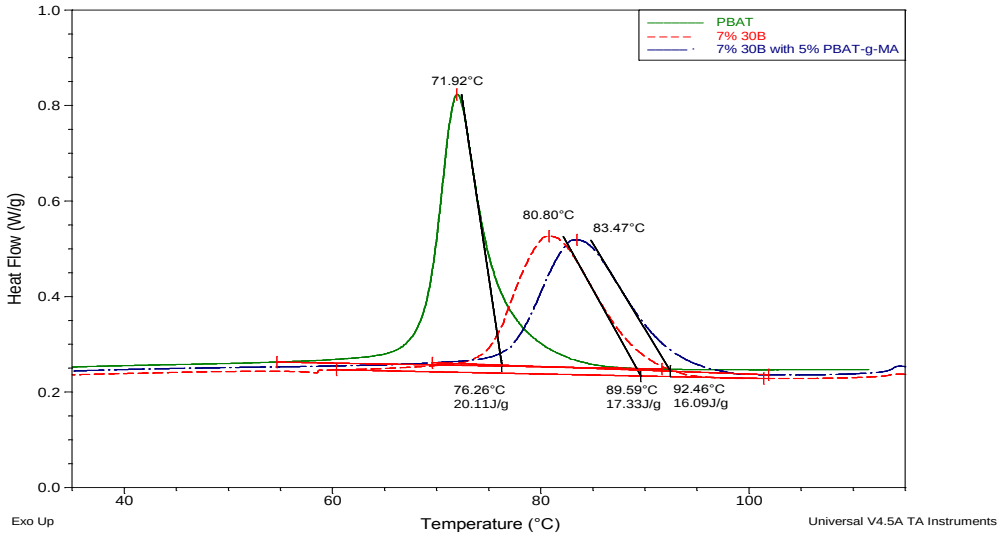


Figure 4.14. Increased Crystallization Temperature in PBAT Nanocomposite with 7 wt% Cloisite 30B

3.8 wt%. Above this clay loading, large agglomerates of clay are formed and the surface-to-volume ratio of the clay is reduced. The compatibilized samples do not display this trend, however, and the crystallization temperatures continue to increase above 5 wt% clay. This indicates that agglomerate formation is reduced due to the reduced interfacial tension between the polymer chains and clay surface, and the mechanism of clay network development has been altered significantly.

The compatibilization of the two composites in Figures 4.13 and 4.14 also generates a broader crystallization peak, which is indicative of a lower overall crystallinity in the sample. The inclusion of clay particles creates barriers which initially nucleate crystal formation but ultimately prevent full crystal growth during cooling, and the addition of maleated PBAT enhances this effect further. Figure 4.16 also shows the reduction in crystallinity associated with the increase in clay concentration. These values were calculated using the reported theroretical value for the enthalpy of 100% crystalline PBAT, 22.3 kJ/mol [70]. The non-compatibilized samples show very little alteration in the extent of crystallization between 1 and 7 wt%. With PBAT-g-MA, the percent crystallinity is decreased further due to the improved exfoliation. Interestingly, the 1 wt% clay composite does not follow this trend. Figure 4.15 shows that the compatibilized 1 wt% composite crystallizes at a higher temperature, but in Figure 4.16 it is apparent that the overall percent crystallinity of the non-compatibilized sample is markedly higher. This is assumed to be due to the increased nucleation sites of the exfoliated tactoids upon compatibilization, but the total number of clay particles is not sufficient to inhibit crystallite growth.

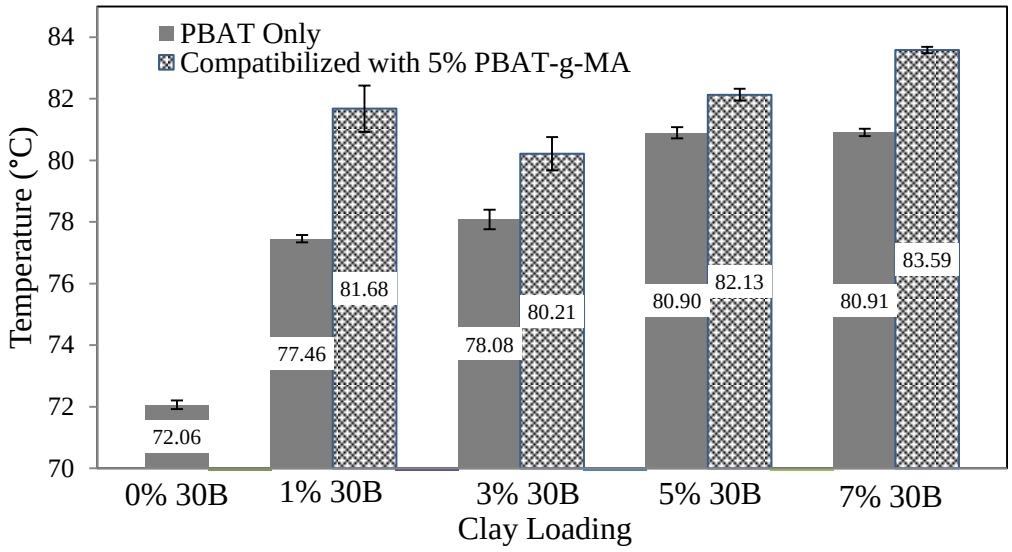


Figure 4.15. Temperature at Maximum Rate of Crystallization of Compatibilized PBAT Nanocomposites

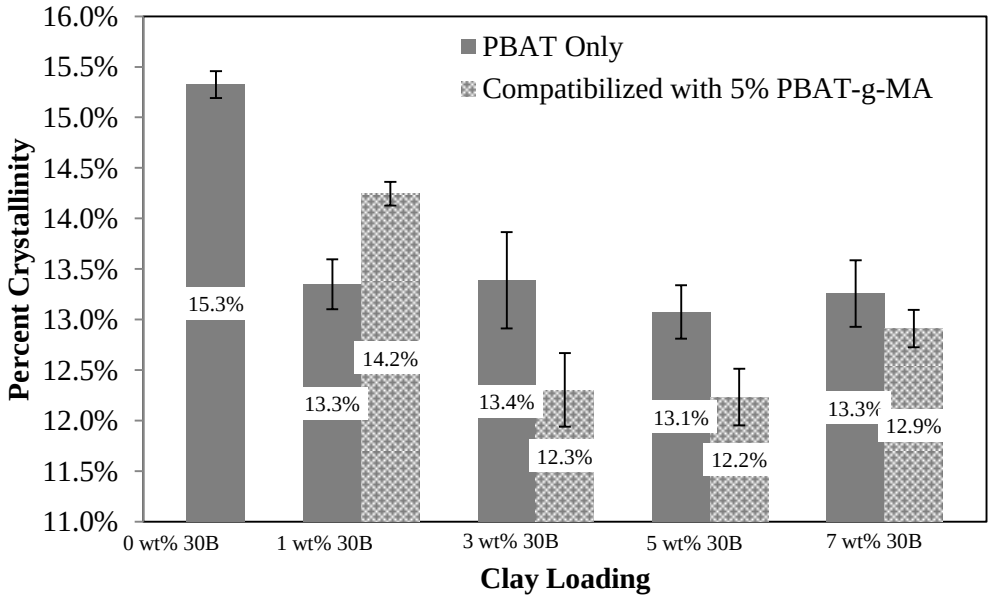


Figure 4.16. Percent Crystallinity Reduction upon PBAT-g-MA Compatibilization (Based on a Theoretical Value for 100% Crystalline PBAT H = 22.3 kJ/mol)

The altered crystallization mechanism has been quantified in literature by the half crystallization time which is given by:

$$t^{\frac{1}{2}} = \frac{T_{Ons} - T_C}{X}$$

where $T_{Ons}$ is the onset temperature of crystallization and $T_C$ is the temperature of maximum crystallization, and $X$ is the cooling rate [71]. This value represents the time until 50% of the sample is crystallized. The average half crystallization times have been calculated for each sample at a cooling rate of 10°C/min and are listed in Table 4.2. Again, the non-compatibilized samples show a decrease in the crystallization rate with increased clay loading until a percolated network is formed at between 3 and 5 wt% clay, and the compatibilized samples were all calculated to have a longer half crystallization time than any of the non-compatibilized samples. This can be attributed to the increased presence of exfoliated clay particles which inhibit ordered chain folding and increase the inhomogeneity in crystallite size.

Table 4.2. Slowed Crystallization Kinetics of Compatibilized PBAT Nanocomposites

| Sample | $t_{1/2}$ (min) | +/- |
|---|---|---|
| 1% 30B | 0.840 | 0.011 |
| 1% 30B Compatibilized | 1.064 | 0.098 |
| 3% 30B | 0.860 | 0.064 |
| 3% 30B Compatiblized | 0.909 | 0.029 |
| 5% 30B | 0.888 | 0.003 |
| 5% 30B Compatibilized | 0.891 | 0.010 |
| 7% 30B | 0.869 | 0.009 |
| 7% 30B Compatibilized | 0.903 | 0.005 |

The exfoliation state of clay influences the mechanism of degradation as greatly as it affects the crystallization in PBAT nanocomposites. The thermogravimetric weight loss curves can therefore provide insight to the enhancement of exfoliation and how the thermal degradation of the material is altered. Figure 4.17 shows the weight loss and derivative weight loss curves for 3 wt% 30B composites with and without PBAT-g-MA relative to the weight loss of neat extruded PBAT during thermal degradation. Close observation reveals that the compatibilized sample exhibits early onset degradation and a higher level of char formation than the specimen without PBAT-g-MA. The summary of these effects for all clay loadings examined can be seen in Figures 4.18 and 4.19. The residue left at 600˚C was increased and the weight loss associated with the thermal

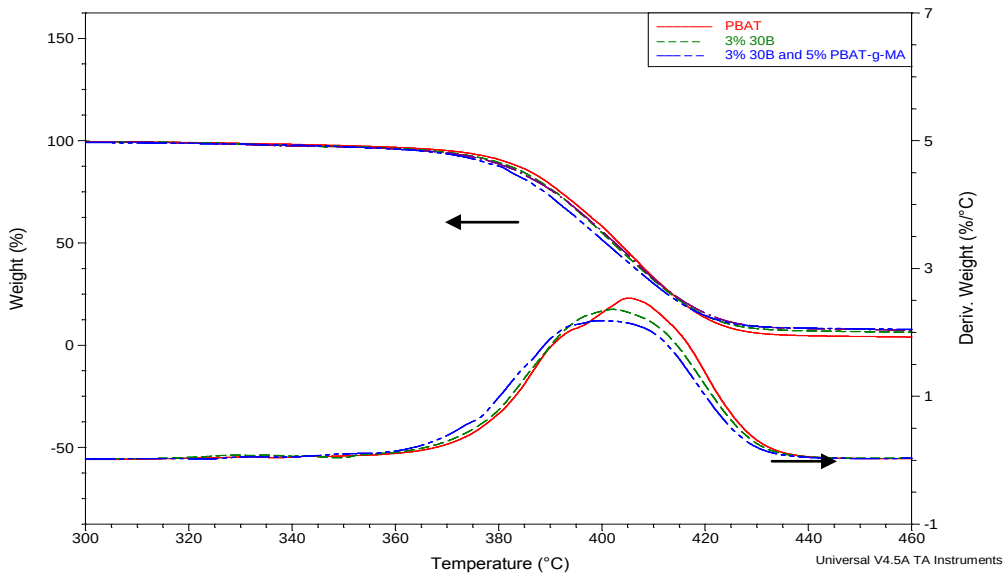


Figure 4.17. Thermogravimetric Curves of 3% 30B Nanocomposites

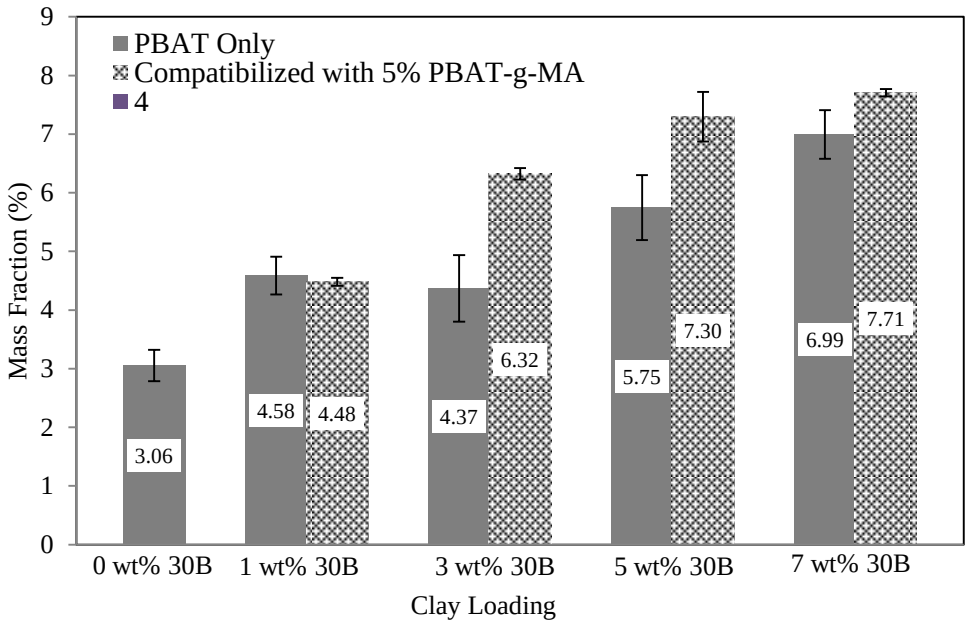


Figure 4.18. Char Residue at 600°C

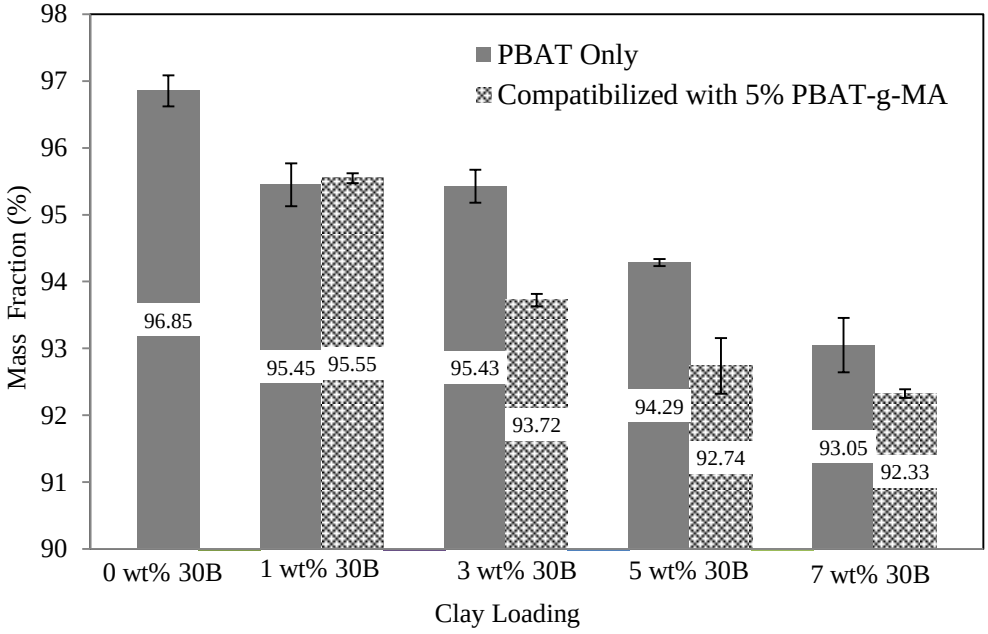


Figure 4.19. Degradation Mass Loss of PBAT Nanocomposites

degradation is reduced with the compatibilizing agent addition. The largest effects are seen at the 3 wt% clay content, where the residue is increased by 45%. This can be credited to the compatibilizer inducing clay percolation below 3 wt% as was observed in the rheological studies. The percolated network limits the transport of degradation products from the sample and increases char formation and flame retardancy [72].

The boosted level of interaction between the polymer chains and the clay surface through compatiblization has also been shown to promote early degradation, leading to char formation and an improved heat barrier to further degradation. Table 4.3 summarizes the 2% weight loss temperatures for all compatibilized samples. The temperature associated with this low level of degradation decreases as clay is incorporated, but these effects are minimized above the experimental percolation threshold of 3.88 wt% and the 5 and 7 wt% composites exhibit similar onset degradation characteristics. The addition of the maleated copolymer renders the increase in clay content more effective at promoting early degradation, and the compatibilized 7 wt% sample shows an average 2% weight loss temperature of 325°C which is nearly 20°C lower than that of neat PBAT.

Table 4.3. Temperature at 2% Sample Weight Loss

| Sample | Temperature °C | +/- °C |
|---|---|---|
| PBAT | 343.3 | 0.8 |
| 1% 30B | 338.6 | 2.6 |
| 1% 30B Compatibilized | 342.9 | 2.0 |
| 3% 30B | 339.2 | 2.9 |
| 3% 30B Compatibilized | 335.9 | 1.3 |
| 5% 30B | 335.8 | 2.6 |
| 5% 30B Compatibilized | 331.4 | 0.9 |
| 7% 30B | 335.1 | 1.7 |
| 7% 30B Compatibilized | 325.3 | 2.8 |

**4.3.6. Tensile Properties.** PBAT can be utilized in compostable film applications because of its ductile nature which yields a high level of elongation before failure. Finding the optimal balance between barrier and elongational properties while improving tensile strength is the driving factor behind the incorporation of nanoclay into PBAT. As clay loading is increased above the percolation threshold without compatibilizer, the tensile modulus is enhanced at the expense of a reduced elongation at break. Figures 4.20 and 4.21 show this trend for non-compatibilized samples with nanoclay content from 1-7 wt%.

When 5% PBAT-g-MA is melt compounded with these nanocomposites the Young's modulus improved for each clay loading examined. The elongation at break is improved for the 5 and 7 wt% samples but the compatibilization causes a decrease in the elongation at break with 3 wt% 30B. While the enhanced exfoliation of clay has been shown to reduce the number of large clay aggregates that result in early failure during tensile tesing, the absolute number of clay particles remains elevated. This can alter the formation mechanism of the PBAT matrix, and the nanocomposite may respond to tensile stress as though the clay content were higher.

The non-compatibilized samples show a significant drop in elongation at break between 3 and 5 wt% 30B, where the percolation threshold was calculated to be. This large decline in elongational properties occurs between 1 and 3 wt% in the compatibilized samples, which correlates to the altered rheological response and crystallization kinetics below 3 wt% suggesting that the percolation threshold for PBAT nanocomposites containing a PBAT-g-MA compatibilizer is also below 3 wt% 30B.

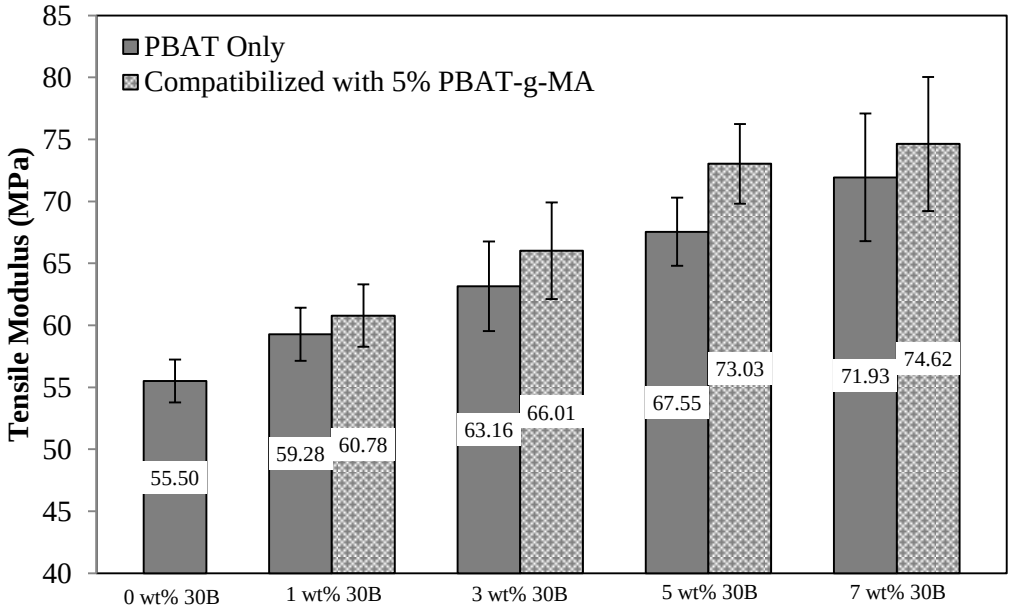


Figure 4.20. Tensile Modulus of Compatibilized PBAT Nanocomposites

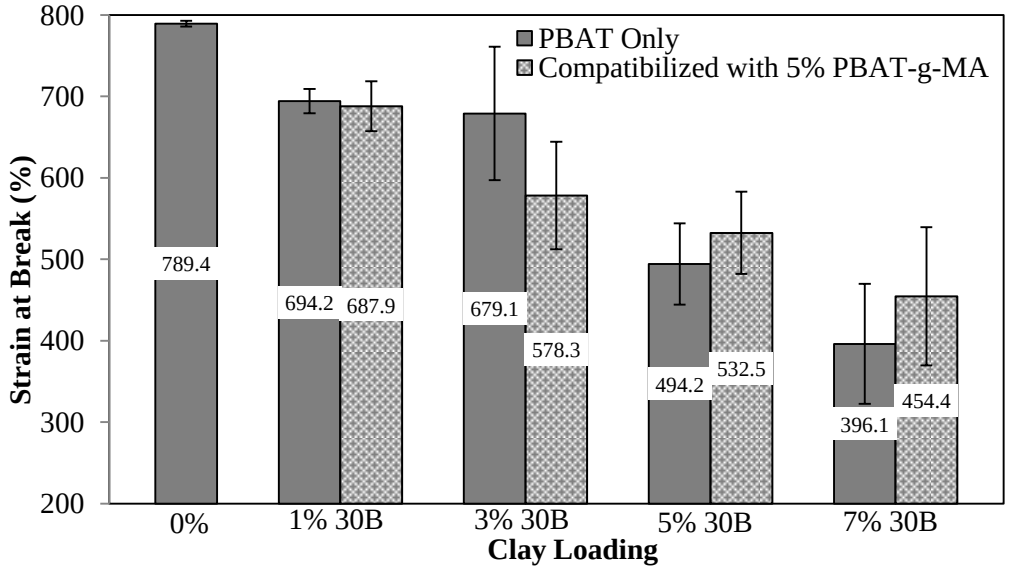


Figure 4.21. Elongation at Break of Compatibilized Nanocomposites

## 4.4. CONCLUSIONS

A compatibilizer that was developed via the free radical maleation of poly(butylene adipate-co-terephthalate) in supercritical carbon dioxide was used to compatibilize PBAT nanocomposites with an organically-modified montmorillonite clay. With only 5 wt% PBAT-g-MA, the exfoliation and dispersion of the nanoclay particles was improved significantly enough to be observed with electron microscopy and x-ray diffraction. While Cloisite 30B has demonstrated a percolation threshold of 3.88 wt% in PBAT, the PBAT nanocomposites with the added compatibilizer demonstrated the thermal behavior and rheological response evident of the development of a secondary filler network between 1 and 3 wt% clay. Both degradation and crystallization was promoted at faster rates initially, but an overall lower percent of crystallization was measured in the compatibilized composites and the char residue after thermal degradation was increased with the incorporation of maleated PBAT. The water vapor transmission rate through the compatibilized films and tensile properties were also significantly improved through the enhanced clay exfoliation. Thus, this solvent-free graft copolymerization method can provide a compatiblizer which is capable of optimizing these properties for PBAT film applications.

# 5. CONCLUSIONS

PBAT nanocomposite films have a wide range of applications in biodegradable packaging, particularly if the nanocomposite can be developed with high compatibility between the PBAT phase and the nanofiller. Graft copolymers are commonly used as a compatibilizing agent to improve the dispersion of a filler in a polymer matrix. In this work, a graft copolymer was developed as a compatibilizer between the PBAT matrix and the nanoclay particles. PBAT-g-MA was prepared via free radical supercritical carbon dioxide grafting, which provided an improved grafting efficiency at lower temperatures and shear than typical melt or solution grafting processes. The maleation reaction was quantified after affixing benzylamine to the anhydride functionality to facilitate spectroscopic analysis. A graft level of 1.16-1.63% was calculated and the optimal operating temperature range was defined as 75-85°C and 80-90°C for BPO and AIBN initiation, respectively.

The effectiveness of such a compatibilizing agent cannot be determined without first fully characterizing the nanocomposite through structure-property analysis. PBAT-Cloisite 30B nanocomposites were prepared via melt extrusion and TEM imaging and x-ray diffraction were used to analyze the structure of the clay particles. Water vapor permeation studies helped to determine the optimal clay loading for barrier property improvement, between 2 and 5 weight percent. The storage and loss modulus curves measured with polymer melt rheology exhibited a developed nanostructure which was destroyed with high frequency shear. From storage modulus values at various clay loading, the percolation threshold was determined to be 3.88 weight percent clay without the presence of a compatibilizer.

The final stage of this research involved incorporating PBAT-g-MA into PBAT nanocomposites to determine the effects on the clay exfoliation and the percolation of the nanoparticles. The viscoelastic and thermal behavior of the compatibilized products indicated that a nanostructure was developed between 1 and 3 weight percent clay, a clay loading significantly below the previously estimated percolation threshold. The enhanced clay exfoliation visible through TEM imaging further supported this lowered percolation threshold. Foremost, the water vapor transmission rates measured through the compatibilized films were markedly lower and the improved elongational properties indicated an enhanced compatibility between the clay and the PBAT matrix as well as a reduction in clay tactoid number and size. Thus, this solvent-free graft copolymerization method provided a compatiblizer which is capable of optimizing the barrier, tensile, and thermal properties of biodegradable PBAT nanocomposite films and widen their range of end-use applications.

# BIBLIOGRAPHY


[1] Al-Salem, S. M., P. Lettieri, and J. Baeyens. "Recycling and Recovery Routes of Plastic Solid Waste (PSW): A Review." Waste Management, 29.10 (2009), 2625-43.

[2] Sorrentino, A., G. Gorrasi, and V. Vittoria. "Potential Perspectives of Bio-Nanocomposites for Food Packaging Applications." Trends in Food Science & Technology, 18.2 (2007), 84-95.

[3] Bastioli, Catia. Handbook of Biodegradable Polymers. Rapra Technology Limited, 2005.

[4] Yoshitsugu Kojima, Arimitsu Usuki, Masaya Kawasumi, Akane Okada, Yoshiaki Fukushima, Toshio Kurauchi and Osami Kamigaito. "Mechanical Properties of Nylon 6-Clay Hybrid." Journal of Materials Research, 8 (1993), 1185-89.

[5] Emmerich, Katja, Felicitas Wolters, and Guenter Kahr. "Clay Profiling: The Classification of Montmorillonites." Clays and Clay Minerals, 57.1 (2009), 104-14.

[6] Whitley, Heather and David Smith, "Free Energy, Energy, and Entropy of Swelling in Cs–, Na–, and Sr– Montmorillonite Clays." Journal of Chemical Physics, 120.11 (2004), 5387-95.

[7] Ingram, Sharon, Hugh Dennis, Ian Hunter, John J. Liggat, Craig, McAdam, and Richard Pethrick. "Influence of Clay Type on Exfoliation, Cure and Physical Properties of in Situ Polymerised Poly(Methyl Methacrylate) Nanocomposites." Polymer International, 57.10 (2008), 1118-27.

[8] Tsai, T., Wen, C., Chuang, H., Lin, M., and Ray, U. "Effect of Clay with Different Cation Exchange Capacity on the Morphology and Properties of Poly(Methyl Methacrylate)/Clay Nanocomposites." Polymer Composites, 30.11 (2009), 1552-1561.

[9] Chavarria, F., et al. "Morphology and Properties of Nanocomposites from Organoclays with Reduced Cation Exchange Capacity." Journal of Applied Polymer Science, 105.5 (2007), 2910-24.

[10] Mohanty, Smita, and Sanjay K. Nayak. "Effect of Clay Exfoliation and Organic Modification on Morphological, Dynamic Mechanical, and Thermal Behavior of Melt-Compounded Polyamide-6 Nanocomposites." Polymer Composites, 28.2 (2007), 153-62.

[11] Al-Khanbashi, Abdullah, Maisa El-Gamal, and Abdelsamie Moet. "Reduced Shrinkage Polyester/Montmorillonite Nanocomposite." Journal of Applied Polymer Science, 98.2 (2005), 767-73.

[12] Witt, W.; Muller, R.J.; Deckwer, W.D. "Biodegradation Behavior and Material Properties of Aliphatic-Aromatic Polyesters of Commercial Importance." Journal Polym. Environment, 5.2 (1997), 81-9.

[13] Rantze, E.; Kleeberg, I.; Witt, U.; Muller, R.J.; Deckwer, W.D. "Aromatic Components in Copolyesters: Model Structures Help to Understand Biodegradability." Macromolecular Symposium, 130.1 (1998), 319-26.

[14] Baniassadi, Majid, Akbar, Ghazavizadeh, Yves Remond, Said Ahzi, David Ruch, and Hamid Garmestani. "Qualitative Equivalence between Electrical Percolation Threshold and Effective Thermal Conductivity in Polymer/Carbon Nanocomposites." Journal of Engineering Materials and Technology, 134.1 (2012), 010902-5.

[15] Al-Saleh, Mohammed H., and Uttandaraman Sundararaj. "An Innovative Method to Reduce Percolation Threshold of Carbon Black Filled Immiscible Polymer Blends." Composites Part A: Applied Science and Manufacturing, 39.2 (2008), 284-93.

[16] Eken, A.E., E.J. Tozzi, D.J. Klingenberg, and W. Bauhofer. "A Simulation Study on the Combined Effects of Nanotube Shape and Shear Flow on the Electrical Percolation Thresholds of Carbon Nanotube/Polymer Composites." Journal of Applied Physics, 109.8 (2011), 084342-9.

[17] Bauhofer, Wolfgang, and Josef Z. Kovacs. "A Review and Analysis of Electrical Percolation in Carbon Nanotube Polymer Composites." Composites Science and Technology, 69.10 (2009), 1486-98.

[18] Kim, Yeon Seok, John B. Wright, and Jaime C. Grunlan. "Influence of Polymer Modulus on the Percolation Threshold of Latex-Based Composites." Polymer, 49.2 (2008), 570-8.

[19] Rzayev, Z.M.O. "Graft Copolymers of Maleic Anhydride and Its Isostructural Analogues: High Performance Engineering Materials." Physics: Chemical Physics, (2011).

[20] Pompe, Tilo, Stefan Zschoche, Nicole Herold, Katrin Salchert, Marie-Francoise Gouzy, Claudia Sperling, Carstern Werner. "Maleic Anhydride Copolymers A Versatile Platform for Molecular Biosurface Engineering." Biomacromolecules, 4.4 (2003), 1072.

[21] Cao, Chengbo, Fanglian Zhu, Xueli Yu, Qin Wang, Chuandong Wang, Baolu Li, Ronghui Lv, and Musen Li. "Two-Step Modification of Poly(D, L-Lactic Acid) by Ethylenediamine-Maleic Anhydride." Biomedical Materials, 3.1 (2008), 015002.

[22] Pompe, Tilo, Kristin Keller, Gisela Mothes, Mirko Nitschke, Mark Teese, Ralf Zimmerman, and Carsten Werner. "Surface Modification of Poly(Hydroxybutyrate) Films to Control Cell–Matrix Adhesion." Biomaterials, 28.1 (2007), 28-37.

[23] Gunning, M. A., O. M. Istrate, L. M. Geever, J. G. Lyons, P. Blackie, B. Chen, and C. L. Higginbotham. "The Effect of Maleic Anhydride Grafting Efficiency on the Flexural Properties of Polyethylene Composites." Journal of Applied Polymer Science, 124.6 (2012), 4799-808.

[24] Petersson, L., K. Oksman, and A. P. Mathew. "Using Maleic Anhydride Grafted Poly(Lactic Acid) as a Compatibilizer in Poly(Lactic Acid)/layered-Silicate Nanocomposites." Journal of Applied Polymer Science, 102.2 (2006), 1852-62.

[25] Kim, Hee-Soo, Byoung-Ho Lee, Sena Lee, Hyun-Joong Kim, and John Dorgan. "Enhanced Interfacial Adhesion, Mechanical, and Thermal Properties of Natural Flour-Filled Biodegradable Polymer Bio-Composites." Journal of Thermal Analysis & Calorimetry, 104.1 (2011), 331-38.

[26] Tserki, V., P. Matzinos, and C. Panayiotou. "Effect of Compatibilization on the Performance of Biodegradable Composites using Cotton Fiber Waste as Filler." Journal of Applied Polymer Science, 88.7 (2003), 1825-35.

[27] Thirmizir, M. Z. Ahmad, Z. A. Mohd Ishak, R. M. Taib, S. Rahim, and S. Mohamad Jani. "Kenaf-Bast-Fiber-Filled Biodegradable Poly(Butylene Succinate) Composites: Effects of Fiber Loading, Fiber Length, and Maleated Poly(Butylene Succinate) on the Flexural and Impact Properties." Journal of Applied Polymer Science, 122.5 (2011), 3055-63.

[28] Lee, Jae Bok, Yun Kyun Lee, Gi Dae Choi, Sang Wook Na, Tae Sung Park, and Woo Nyon Kim. "Compatibilizing Effects for Improving Mechanical Properties of Biodegradable Poly (Lactic Acid) and Polycarbonate Blends." Polymer Degradation and Stability, 96.4 (2011), 553-60.

[29] Zhang, Cai-Liang, Lian-Fang Feng, Xue-Ping Gu, Sandrine Hoppe, and Guo-Hua Hu. "Efficiency of Graft Copolymers as Compatibilizers for Immiscible Polymer Blends." Polymer, 48.20 (2007), 5940-9.

[30] Kanzawa, Takeshi, and Katsuhisa Tokumitsu. "Mechanical Properties and Morphological Changes of Poly(Lactic Acid)/Polycarbonate/Poly(Butylene Adipate-Co-Terephthalate) Blend through Reactive Processing." Journal of Applied Polymer Science, 121.5 (2011), 2908-18.

[31] Takamura, Masumi, Tomoyuki Nakamura, Tatsuhiro Takahashi, and Kiyohito Koyama. "Effect of Type of Peroxide on Cross-Linking of Poly(l-Lactide)." Polymer Degradation and Stability, 93.10 (2008), 1909-16.

[32] Moad,Graeme; Solomon, David H. The Chemistry of Radical Polymerization. 2nd ed. Boston: Elsevier, 2006.

[33] Fink, Johannes Karl. Reactive Polymers Fundamentals and Applications - A Concise Guide to Industrial Polymers. William Andrew Publishing/Plastics Design Library (2005).

[34] Denisov, E. T., T.G. Denisova, and T. S. Pokidova. Handbook of Free Radical Initiators. John Wiley & Sons, Inc: Hoboken, NJ (2003).

[35] Pan, Bo, Kalyanaraman Viswanathan, Charles E. Hoyle, and Robert B. Moore. "Photoinitiated Grafting of Maleic Anhydride onto Polypropylene." Journal of Polymer Science Part A: Polymer Chemistry, 42.8 (2004), 1953-62.

[36] Deng, J., L. Wang, L. Lie, and W. Yang. "Developments and New Applications of UV-Induced Surface Graft Polymerizations." Progress in Polymer Science, 34 (2009), 156-93.

[37] Morris, R. E., A. E. Mera, and R. F. Brady Jr. "Development of a Model System to Study Fuel Autoxidation in Supercritical Media: Decompositions Kinetics of 2,2'-Azobis(Isobutyronitrile) in Supercritical Carbon Dioxide." Fuel, 79 (2000) 1101-7.

[38] Braun, Dietrich. "Origins and Development of Initiation of Free Radical Polymerization Processes." International Journal of Polymer Science, (2009).

[39] Lin, S., J. Yang, J. Yan, Y. Zhao, and B. Yang. "Sorption and Diffusion of Supercritical Carbon Dioxide in a Biodegradable Polymer." Journal of Macromolecular Science Physics, 49.2 (2010), 286-300.

[40] Lee, S., S. Kwak, and F.O. Azzam. "Graft Copolymerization in Supercritical Fluid Media." U.S. Patent No. 5,663,237, September 2, 1997.

[41] Clark, K., and S. Lee, "Removal of Ungrafted Monomer from Polypropylene-graft-Maleic Anhydride via Supercritical Carbon Dioxide Extraction," Polymer Engineering & Science, 44.9 (2004), 1636-42.

[42] Paul, D. R., and L. M. Robeson. "Polymer Nanotechnology: Nanocomposites." Polymer, 49.15 (2008), 3187-204.

[43] Cassagnau, Ph. "Melt Rheology of Organoclay and Fumed Silica Nanocomposites." Polymer, 49.9 (2008), 2183-96.

[44] Lee, Y.H. C.B. Park, M. Sain, M. Kontopoulou, W.J. Zheng, "Effects of Clay Dispersion and Content on the Rheological, Mechanical Properties, and Flame Retardance of HDPE/Clay Nanocomposites." Journal of Applied Polymer Science, 105.4 (2007), 1993-9.

[45] Akcora, Pinar, Sanat K. Kumar, Victoria Garcia Sakai, Yu Li, Brian C Benicewicz, and Linda S. Schadler. "Segmental Dynamics in PMMA-Grafted Nanoparticle Composites." Macromolecules, 43.19 (2010), 8275–81.

[46] Berta, M., A. Saiani, C. Lindsay, and R. Gunaratne. "Effect of Clay Dispersion on the Rheological Properties and Flammability of Polyurethane-Clay Nanocomposite Elastomers." Journal of Applied Polymer Science 112.5 (2009): 2847-53.

[47] Galgali, Girish, C. Ramesh, and Ashish Lele. "A Rheological Study on the Kinetics of Hybrid Formation in Polypropylene Nanocomposites." Macromolecules, 34.4 (2001), 852-8.

[48] Song, Yihu, and Qiang Zheng. "Linear Viscoelasticity of Polymer Melts Filled with Nano-Sized Fillers." Polymer, 51.14 (2010), 3262-8.

[49] Shahlari, Mahin. "Biodegradable Polymer/Clay Nanocomposites Based on Poly(Butylene Adipate-co-Terephthalate and Polylactide." Ph.D. Dissertation, Missouri University of Science and Technology, (2011).

[50] Huihua, Liu, Deeptangshu Chaudhary, Shin-ichi Yusa, and Moses O. Tade. "Glycerol/Starch/Na+-Montmorillonite Nanocomposites: A XRD, FTIR, DSC and 1H NMR Study." Carbohydrate Polymers, 83.4 (2011), 1591-7.

[51] Qian, Zhongzhong, Hu Zhou, Xinfeng Xu, Yanfen Ding, Shimin Zhang, and Minghu Yang. "Effect of the Grafted Silane on the Dispersion and Orientation of Clay in Polyethylene Nanocomposites." Polymer Composites, 30.9 (2009), 1234-442.

[52] Eckel, Deborah F., Michael P. Balogh, Paula D. Fasulo, and William R. Rodgers. "Assessing Organo-clay Dispersion in Polymer Nanocomposites." Journal of Applied Polymer Science, 93.3 (2004), 1110-7.

[53] Choudalakis G., and A. D. Gotsis. "Permeability of Polymer/Clay Nanocomposites: A Review." European Polymer Journal, 45.4 (2009), 967-84.

[54] Gorrasi, Giuliana, Mariarosaria Tortora, Vittoria Vittoria, Dirk Kaempfer, and Rolf Mulhaupt. "Transport Properties of Organic Vapors in Nanocomposites of Organophilic Layered Silicate and Syndiotactic Polypropylene." Polymer, 44.13 (2003), 3679-3685.

[55] Wu, Defeng, Chixing Zhou, and Ming Zhang. "Rheology of Isothermally Crystallized Poly(Butylene Terephthalate) Nanocomposites with Clay Loadings Under the Percolation Threshold." Journal of Polymer Science Part B: Polymer Physics, 45.2 (2007), 229-38.

[56] Eslami, H. and M. Grmela. "Linear and Nonlinear Rheology of Polymer Layered Silicate Nanocomposites." Journal of Rheology, 54.3 (2010), 539-62.

[57] Chivrac, F., E. Pollet, and L. Avérous. "Nonisothermal Crystallization Behavior of Poly(Butylene Adipate-co-Terephthalate)/Clay Nano-Biocomposites." Journal of Polymer Science Part B: Polymer Physics, 45.13 (2007), 1503-10.

[58] Torre, L., J. M. Kenny and A. M. Maffezzoli. "Degradation Behavior of a Composite Material for Thermal Protection Systems Part I-Experimental Characterization." Journal of Materials Science, 33.12 (1998), 3137-43.

[59] Coltelli, Maria-Beatrice, Simona Bronco, and Carlos Chinea. "The Effect of Free Radical Reactions on Structure and Properties of Poly(Lactic Acid) (PLA) Based Blends." Polymer Degradation and Stability, 95.3 (2010), 332-41.

[60] Moad, Graeme. "Chemical Modification of Starch by Reactive Extrusion." Progress in Polymer Science, 36.2 (2011), 218-37.

[61] Luque de Castro, M. D., and F. Priego-Capote. "Soxhlet Extraction: Past and Present Panacea." Journal of Chromatography A, 1217.16 (2010), 2383-9.

[62] Xu, Qun, Zhenzhong Hou, Guangfa Zhang, Haijuan Fan, Jianbo Li, and Shijun Zheng. "Supercritical Carbon Dioxide Assisted Grafting of Polyacrylamide to Polypropylene." Journal of Applied Polymer Science, 101.4 (2006), 2614-8.

[63] Luo, Yanfeng, Yuanliang Wang, Xufeng Niu, and Juanfang Shang. "Synthesis, Characterization and Biodegradation of Butanediamine-Grafted Poly(Dl-Lactic Acid)." European Polymer Journal, 43.9 (2007), 3856-64.

[64] Hu, G. H., and J. T. Lindt. "Amidification of Poly(Styrene-Co-Maleic Anhydride) with Amines in Tetrahydrofuran Solution: A Kinetic Study." Polymer Bulletin, 29.3 (1992), 357-63.

[65] Trivedi, Akshay H., Soonjong Kwak, and Sunggyu Lee. "Grafting of Poly(Vinyl Chloride) and Polypropylene with Styrene in a Supercritical $CO_2$ Solvent Medium: Synthesis and Characterization." Polymer Engineering and Science, 41.11 (2001), 1923.

[66] Guan, Z., J.R. Combes, Y.Z. Mencelogln, and J.M. DeSimone. "Homogenous Free Radical Polymerizations in Supercritical Carbon Dioxide: Thermal Decomposition of 2,2'-Azobis(Isobutyronitrile)." Macromolecules, 26 (1993), 2663.

[67] Zhang, Ronghua, Yutian Zhu, Jianguo Zhang, Wei Jiang, and Jinghua Yin. “Effect of the Initial Maleic Anhydride Content on the Grafting of Maleic Anhydride Onto Isotactic Polypropylene.” Journal of Polymer Science Part A: Polymer Chemistry, 43.22 (2005), 5529-34.

[68] Pong, Sheng-Hong, Chuan-Pin Lu, Ming-Chih Wang, Shih-Hsuan Chiu. “Polypropylene Degradation Control During Reactive Extrusion.” Journal of Applied Polymer Science, 95.2 (2005), 280-9.

[69] Parent, J. Scott, Aidan Bodsworth, Saurav S. Sengupta, Marianna Kontopoulou, Bharat I. Chaudhary, Drew Poche, and Stephane Cousteaux. "Structure–rheology Relationships of Long-Chain Branched Polypropylene: Comparative Analysis of Acrylic and Allylic Coagent Chemistry." Polymer, 50.1 (2009), 85-94.

[70] Chivrac, Frederic; Kadlecova, Zuzana; Pollet, Eric; Averous, Luc. “Aromatic Copolyester-Based Nanobiocomposites: Elaboration, Structural Characterization and Properties.” Journal of Polymers and the Environment, 14 (2006), 393-401.

[71] Chen, Jung-Hung, Chin-Chi Chen, and Ming-Chien Yang. “Characterization of Nanocomposites of Poly(Butylene Adipate-co-Terephthalate) Blending with Organoclay.” Journal of Polymer Research, 18.6 (2011), 2151-59.

[72] Lim, S.T., Y.H. Hyun, H.J. Choi, and M.S. Jhon. “Synthetic Biodegradable Aliphatic Polyester/Montmorillonite Nanocomposites.” Chemistry of Materials, 14 (2002), 1839–44.

# VITA

Alexandria Niemoeller was born in Saint Louis, Missouri. In May 2007 she received her B.S. with Honors and Cum Laude in Chemical Engineering from the University of Missouri – Columbia. She began undergraduate research work in January 2006 in the area of supercritical water reformation of hydrocarbon fuels for the production of hydrogen. In August 2007 she joined a graduate research team at the Missouri University of Science and Technology with the Chancellor's Fellowship for Chemical Engineering and began work in the field of biodegradable polymer processing and characterization. She was awarded the U.S. Department of Education's GAANN Fellowship in June 2010. From August 2010 to July 2012 she completed her research as a visiting scholar at the Sustainable Energy and Advanced Materials Laboratory of Ohio University in Athens, Ohio.

She has been a member of the American Institute of Chemical Engineers (AIChE) and Society of Plastics Engineers since 2006 and 2008, respectively. She was inducted into the Chemical Engineering Honor Society, Omega Chi Epsilon, in 2006 and served as the group's president from August 2006 to May 2007.